

# The Stromlo-APM Redshift Survey III. Redshift Space Distortions, Omega and Bias

**J. Loveday**

Fermi National Accelerator Laboratory, PO Box 500, Batavia, IL 60510, USA  
loveday@fnal.gov

**G. Efstathiou**

Department of Physics, Keble Road, Oxford, OX1 3RH, England  
g.efstathiou@physics.oxford.ac.uk

**S.J. Maddox**

Royal Greenwich Observatory, Madingley Road, Cambridge, CB3 0EZ, England  
sjm@mail.ast.cam.ac.uk

**B.A. Peterson**

Mount Stromlo and Siding Spring Observatories, Weston Creek PO, ACT 2611, Australia  
peterson@mso.anu.edu.au

Revised February 26, 1996

## Abstract

Galaxy redshift surveys provide a distorted picture of the universe due to the non-Hubble component of galaxy motions. By measuring such distortions in the linear regime one can constrain the quantity  $\beta = \Omega^{0.6}/b$  where  $\Omega$  is the cosmological density parameter and  $b$  is the (linear) bias factor for optically-selected galaxies. In this paper we apply two techniques for estimating  $\beta$  from the Stromlo-APM redshift survey — (1) measuring the anisotropy of the redshift space correlation function in spherical harmonics and (2) comparing the amplitude of the direction-averaged redshift space correlation function to the real space correlation function. We test the validity of these techniques, particularly whether the assumption of linear theory is justified, using two sets of large  $N$ -body simulations. We find that the first technique is affected by non-linearities on scales up to  $\sim 30h^{-1}\text{Mpc}$ . The second technique is less sensitive to non-linear effects and so is more useful for existing redshift surveys.

The Stromlo-APM survey data favours a low value for  $\beta$ , with  $\beta \lesssim 0.6$ . A bias parameter  $b \approx 2$  is thus required if  $\Omega \equiv 1$ . However, higher-order correlations measured from the APM galaxy survey (Gaztañaga and Frieman 1994) indicate a low value for the bias parameter  $b \approx 1$ , requiring that  $\Omega \lesssim 0.5$ . We also measure the relative bias for samples of galaxies of various luminosity and morphological type and find that low-luminosity galaxies are roughly three times less biased than  $L^*$  galaxies. For the galaxy population as a whole, we measure a real space variance of galaxy counts in  $8h^{-1}\text{Mpc}$  spheres of  $(\sigma_8^2)_g = 0.89 \pm 0.05$ .

Subject headings: galaxies: clustering — galaxies: distances and redshifts — galaxies: fundamental parameters — large-scale structure of universe — surveys

# 1 Introduction

Galaxy redshift surveys can provide some of the most important constraints on theories of large-scale structure, but they must be analysed with care. For pure, unperturbed Hubble flow, galaxy clustering measured in redshift space would be isotropic and identical to that measured in real space. However, in practice, peculiar velocities will distort the redshift space correlation function. Since the amplitude of peculiar velocities depends on the cosmological density parameter  $\Omega$ , measurements of this distortion can constrain the value of  $\Omega$ . On small scales, the effect of peculiar velocities is to elongate clusters of galaxies along the line of sight in redshift space, leading to the well known ‘fingers of God’. However, on large scales, coherent bulk flows dominate the peculiar velocity field resulting in a *compression* in the clustering pattern along the line of sight. This effect is easily seen in the Stromlo-APM Survey as shown in Figure 1, which is a contour plot of the full redshift space correlation function  $\xi(\sigma, \pi)$  as a function of components of separation parallel ( $\pi$ ) and perpendicular ( $\sigma$ ) to the line of sight. A compression of the low-amplitude  $\xi$  contours in the  $\pi$  direction compared with the  $\sigma$  direction is clearly visible for  $\pi \gtrsim 10h^{-1}\text{Mpc}$ . (We assume a Hubble constant of  $H_0 = 100h \text{ km/s/Mpc}$ .)

This large-scale anisotropy in redshift space clustering is most naturally expressed in terms of the power spectrum. Kaiser (1987) has shown that in the linear regime of gravitational instability models, the power spectra in redshift space,  $P_s(\mathbf{k})$  and real space  $P_r(\mathbf{k})$  are simply related by

$$P_s(\mathbf{k}) = (1 + \beta\mu_{\mathbf{k}}^2)^2 P_r(\mathbf{k}), \quad (1)$$

where  $\mu_{\mathbf{k}}$  is the cosine of the angle between the wavevector  $\mathbf{k}$  and the line of sight. The amplitude of the distortion is determined by the parameter  $\beta = f(\Omega)/b$ , where  $f(\Omega) \approx \Omega^{0.6}$  is the dimensionless growth rate of growing modes in linear theory. The bias parameter  $b$  relates the fluctuations in galaxy density to the underlying mass density in the linear regime,  $\delta_g = b\delta_\rho$  for linear bias. Several practical methods for measuring  $\beta$  have recently been applied: measuring the anisotropy of the correlation function (Hamilton 1992, 1993a; Fisher *et al.* 1994a), the anisotropy of the power spectrum (Cole, Fisher and Weinberg 1994, 1995; Tadros and Efstathiou 1996) and spherical harmonics of the density field (Fisher *et al.* 1994b; Heavens and Taylor 1995).

We follow the correlation function approach in this paper.<sup>1</sup> Hamilton (1992) has pointed out that the cosine  $\mu_{\mathbf{k}}$  in Fourier space transforms to an operator in real space:

$$\xi_s(r, \mu) = [1 + \beta(\partial/\partial z)^2(\nabla^2)^{-1}]^2 \xi_r(r), \quad (2)$$

where  $(\nabla^2)^{-1}$  denotes the inverse Laplacian operator and  $\mu = \hat{\mathbf{r}} \cdot \hat{\mathbf{z}}$  is the cosine angle between pair separation  $\mathbf{r}$  and the line of sight  $\mathbf{z}$ . The redshift space correlation function  $\xi_s(r, \mu)$  is conveniently expressed as a sum of spherical harmonics involving the first three even-order Legendre polynomials, (the odd-order harmonics vanish by pair-exchange symmetry)

$$\xi_s(r, \mu) = \xi_0(r)P_0(\mu) + \xi_2(r)P_2(\mu) + \xi_4(r)P_4(\mu). \quad (3)$$

Hamilton gives expressions for the  $\xi_i(r)$  in terms of integrals over  $\xi_r(r)$  [his equations (6)–(9)].

To solve the inverse problem, *i.e.* to go from redshift space clustering to real space clustering, Hamilton integrates the equations describing the real and redshift space correlation functions over

---

<sup>1</sup> For a power spectrum analysis of the Stromlo-APM survey, see Tadros and Efstathiou (1996).

planes normal to the vector  $\mathbf{r}$  at separation  $r$ , expands in spherical harmonics and differentiates with respect to  $r$ . He thereby obtains an explicit expression for  $\beta$  and  $\xi_r(r)$  in terms of the harmonics  $\xi_l(r)$  of the redshift space correlation function. Further volume averaging to minimize cancelation of terms finally results in an equation for  $\beta$  involving the 0th and 2nd order harmonics of the redshift space correlation function:

$$\frac{1 + \frac{2}{3}\beta + \frac{1}{5}\beta^2}{\frac{4}{3}\beta + \frac{4}{7}\beta^2} = \frac{\xi_0(r) - 3 \int_0^r \xi_0(s)(s/r)^3 ds/s}{\xi_2(r)}. \quad (4)$$

One can also write a similar expression involving the 2nd and 4th order harmonics, but in practice, the 4th order harmonic is too noisy and too strongly affected by non-linear effects to be useful.

As well as causing anisotropy in redshift space, large-scale streaming motions also produce an amplification in the direction-averaged redshift space correlation function on large scales. For fluctuations in the linear regime, the direction-averaged redshift space correlation function  $\xi(s)$  and the real space correlation function  $\xi(r)$  are related by (Kaiser 1987)

$$\xi(s) \approx \left(1 + \frac{2}{3}\beta + \frac{1}{5}\beta^2\right) \xi(r). \quad (5)$$

The large uncertainty in the value of  $\beta$  hinders comparison of  $\xi(s)$  with real space predictions of galaxy clustering from various models (see, for example, Loveday *et al.* 1992a). In a recent paper (Loveday *et al.* 1995, hereafter Paper 2), we estimated the real-space correlation function of optically-selected galaxies by cross-correlating galaxies in the sparse-sampled Stromlo-APM Redshift Survey with the fully-sampled, parent APM Galaxy Survey. This projected cross-correlation function is unaffected by redshift-space distortions and may be stably inverted to give the real-space correlation function  $\xi(r)$ . Moreover, the large number of cross-pairs enables clustering to be measured to smaller scales than using the redshift survey data alone. If both  $\xi(r)$  and  $\xi(s)$  can be reliably measured in the linear regime then the value of  $\beta$  can be constrained using equation (5).

We assess the relative merits of these two methods of estimating  $\beta$  (equations 4 and 5) by analyzing  $N$ -body simulations. The two sets of simulations, of low and high density, are designed to be similar to the Stromlo-APM data in both the clustering and dynamics of the galaxies. In particular, we estimate the sensitivity of the methods to non-linear dynamics of the galaxy distribution.

The above expressions (1–5) assume a plane-parallel approximation for peculiar displacements. In order to approximate this ideal in our analyses, we use only those pairs of galaxies separated by less than 50 degrees on the sky. This rejects about 20% of galaxy pairs, and, as Cole *et al.* (1994) have demonstrated, will limit deviations from the plane-parallel approximation to no more than a 5% bias in the estimated value of  $\beta$ .

Throughout the paper, we use  $r$  to denote real space separations and  $s$  to denote separations in redshift space. Error bars on measurements from survey data are estimated using the bootstrap resampling technique (Barrow, Bhavsar and Sonoda 1984) with nine bootstrap resamplings of the survey. Error bars for simulations are determined from the variance between ten independent realizations of the low-density model and nine realizations of the high-density model.

The layout of the paper is as follows. The Stromlo-APM survey data and the  $N$ -body simulations are described and compared in §2. In §3 we test the estimators for  $\beta$  using the simulations. In §4 we apply the estimators to the Stromlo-APM data and also present the relative bias and redshift space distortions for different galaxy types. Finally, our conclusions are given in §5.

## 2 Survey Data and N-Body Simulations

Both equations (4) and (5) assume that linear theory is valid on scales on which  $\xi$  can be reliably measured. It is important to test this assumption of linearity before using these equations to estimate  $\beta$ . We do this by analyzing two ensembles of CDM-like  $N$ -body simulations. In this section we describe the Stromlo-APM survey data and the simulations, and show that the simulations mimic the observed clustering and dynamics of the galaxy distribution quite faithfully.

### 2.1 Stromlo-APM Survey Data

The Stromlo-APM redshift survey consists of 1787 galaxies with  $b_J \leq 17.15$  selected randomly at a rate of 1 in 20 from the APM (Automated Plate Measuring) galaxy survey (Maddox *et al.* 1990a,b). The survey covers a solid angle of 1.3 sr (4300 square degrees) in the south galactic cap. The APM magnitudes have been calibrated and corrected for photographic saturation using CCD photometry as described by Loveday *et al.* 1992b (hereafter Paper 1). An approximate morphological type was assigned to each galaxy by visually inspecting the images on the United Kingdom Schmidt Telescope (UKST) survey plates. Redshifts were obtained with the Mount Stromlo-Siding Spring Observatory (MSSSO) 2.3m telescope at Siding Spring. Measured radial velocities were transformed to the local group frame using  $v = v + 300 \sin(l) \cos(b)$  and we assumed  $\Lambda = 0$ ,  $q_0 = 0.5$  and  $H_0 = 100 \text{ km s}^{-1} \text{ Mpc}^{-1}$  with uniform Hubble flow in calculating distances and absolute magnitudes. We adopt  $k$ -corrections for different morphological types in the  $b_J$  system as described by Efstathiou, Ellis and Peterson (1988). More details about the survey are given in Paper 1 and the construction of the survey is described in full by Loveday *et al.* (1996).

### 2.2 Simulations

We use the two sets of  $N$ -body simulations described by Croft and Efstathiou (1994); a low-density CDM model with  $\Omega_0 = 0.2$  and a cosmological constant (LCDM) and a mixed dark matter model with  $\Omega_0 = 1$  (MDM). We analyze ten realizations of the LCDM model and nine realizations of the MDM model. These simulations combine a large volume (box length =  $300h^{-1} \text{ Mpc}$ ) with a force resolution of  $\approx 80h^{-1} \text{ kpc}$  for  $10^6$  particles, and so can be used to generate reasonable approximations to our redshift survey. Both sets of  $N$ -body simulations have enhanced large-scale power compared with the standard CDM model; the LCDM model by having  $\Gamma = \Omega_0 h = 0.2$  and a nonzero cosmological constant  $\lambda = \Lambda / (3H_0^2) = (1 - \Omega_0) = 0.8$  and the MDM model by having  $\Omega_\nu = 0.3$  from neutrinos and  $h = 0.5$ .

In order to generate mock Stromlo-APM catalogues from the simulations, ‘galaxies’ were selected within the APM area and with the Stromlo-APM selection function (Paper 1), such that they traced the mass particles in an unbiased way. This procedure produces mock catalogues of on average 33,500 ‘galaxies’ each. We select a subset of 1 in 20 galaxies at random from each simulated catalogue in order to mimic the sparse sampling strategy of the Stromlo-APM survey. The intrinsic value of  $\beta$  for the simulations is, by construction,  $\beta = 0.38$  for the LCDM simulations and  $\beta = 1$  for the MDM simulations.

## 2.3 Galaxy Clustering in Real and Redshift Space

We estimate the redshift-space correlation functions from the survey and the simulations using the density-independent estimator for  $\xi(s)$  discussed in Paper 2,

$$1 + \xi(s) = \frac{w_{gg}(s)w_{rr}(s)}{[w_{gr}(s)]^2}. \quad (6)$$

Here  $w_{gg}(s)$ ,  $w_{gr}(s)$  and  $w_{rr}(s)$  are the summed products of weights of galaxy-galaxy, galaxy-random and random-random pairs respectively. Note that the relative densities of galaxy and random points measured at separation  $s$  are automatically accounted for by this estimator — there is no need to assume an overall galaxy density  $n_g$ . This estimator, due to Hamilton (1993b), is insensitive to variations in galaxy density and provides a very stable estimate of  $\xi(s)$ .

To calculate the real-space correlation function  $\xi(r)$ , we measure the projected cross-correlation function between the redshift data and the angular data from the fully-sampled parent catalogue,

$$\Xi(\sigma) = \int_{-\infty}^{+\infty} \xi(\sqrt{\Delta y^2 + \sigma^2}) d\Delta y, \quad (7)$$

where the integral extends over all line-of-sight separations  $\Delta y$  for pairs of galaxies with given projected separation  $\sigma = y\theta$  ( $\theta$  is the angular separation and  $y$  is the distance to the galaxy of known redshift). This projected function is inverted numerically to give an estimate of  $\xi(r)$ , which is unaffected by redshift-space distortions. See Saunders *et al.* (1992) and Paper 2 for a detailed description of this estimator.

In Figure 2 we compare the clustering of galaxies in (a) redshift space and (b) real space for the Stromlo-APM survey and for the  $N$ -body simulations. The error bars show the scatter between nine bootstrap resamplings of the survey. The measured variance between the different realizations of the simulations yields similar error bars, which are not plotted here for the sake of clarity. We see that the simulations match the observed clustering of galaxies reasonably well on large scales, although on small scales the LCDM models overpredict and the MDM models underpredict the observed clustering. The plateau in the real-space clustering of Stromlo-APM galaxies at  $r \approx 20\text{--}30h^{-1}\text{Mpc}$  appears to be significant given the size of the random errors. However, as discussed in Paper 2,  $\xi(r)$  inferred from inversion of the projected cross-correlation with the parent catalogue is subject to systematic error beyond  $r \approx 20h^{-1}\text{Mpc}$ , although neither of the simulations shows any feature here. It is clear that we will need to check that we obtain consistent estimates of  $\beta$  on different scales if our results are to be completely trustworthy.

We have fit power-laws to the correlation functions plotted in Figure 2. We fit over the range  $1.5 < s < 30 h^{-1}\text{Mpc}$  in redshift space and  $0.2 < r < 20 h^{-1}\text{Mpc}$  in real space. The parameters to these power-law fits are given in Table 1.

## 2.4 Galaxy Peculiar Velocities

If the  $N$ -body simulations are to be used to check for non-linear effects in the real data, then it is important to compare the amplitude of small-scale, virialized motions in the simulations with those in the data. By comparing estimates of clustering in redshift space and real space, one can constrain the galaxy peculiar velocity distribution  $f(w)$  (eg. Bean *et al.* 1983, Davis and Peebles 1983). The

redshift space correlation function  $\xi(\sigma, \pi)$  is given by convolving the real space correlation function  $\xi(r)$  with  $f(w)$ ,

$$1 + \xi(\sigma, \pi) = \int_{-\infty}^{\infty} [1 + \xi(r)] f[w_3 + H_0 \beta \xi(1 + \xi)^{-1} r_3] dw_3, \quad (8)$$

(Bean *et al.* 1983), where  $r^2 = \sigma^2 + r_3^2$ ,  $r_3 = \pi - w_3/H_0$  (the subscript 3 denotes the line-of-sight component of a vector quantity) and  $\langle w \rangle \approx -H_0 \beta \xi(1 + \xi)^{-1} r_3$  is the mean streaming velocity of galaxies at separation  $r$ .

We have measured  $\xi(\sigma, \pi)$  in four  $\sigma$  bins each of width  $2h^{-1}$ Mpc centred on 1, 3, 5 and  $7h^{-1}$ Mpc — Figures 3*a*, *b* and *c* for the data, LCDM and MDM simulations respectively. We have calculated the best-fit rms peculiar velocity,  $\langle w^2 \rangle^{1/2}$ , for three models for  $f(w)$ , a Gaussian,

$$f(w) = \frac{1}{\sqrt{2\pi} \langle w^2 \rangle^{1/2}} \exp\left(\frac{-w^2}{2\langle w^2 \rangle}\right), \quad (9)$$

a  $|w|^{3/2}$  distribution,

$$f(w) = \frac{0.476}{\langle w^2 \rangle^{1/2}} \exp\left(\frac{-0.7966|w|^{3/2}}{\langle w^2 \rangle^{3/4}}\right), \quad (10)$$

and an exponential distribution,

$$f(w) = \frac{1}{\sqrt{2} \langle w^2 \rangle^{1/2}} \exp\left(\frac{-\sqrt{2}|w|}{\langle w^2 \rangle^{1/2}}\right). \quad (11)$$

The optimum value of  $\langle w^2 \rangle^{1/2}$  for each distribution was calculated by maximizing the likelihood

$$\mathcal{L} = \prod_{\pi\text{-bins}} [2\pi \text{Var}\{\xi(\sigma, \pi)\}]^{-1/2} \exp\left[\frac{-(\xi^o(\sigma, \pi) - \xi^p(\sigma, \pi))^2}{2\text{Var}\{\xi(\sigma, \pi)\}}\right], \quad (12)$$

where  $\xi^o(\sigma, \pi)$  is the observed redshift space correlation function,  $\text{Var}\{\xi(\sigma, \pi)\}$  is the observed variance in  $\xi^o(\sigma, \pi)$  from bootstrap resampling (or from different realizations of the simulations) and  $\xi^p(\sigma, \pi)$  is the predicted correlation function from (8). We use the measured  $\xi(r)$  from Figure 2(b) in equation (8) and substitute  $\beta = 0.38$  and  $\beta = 1$  for the LCDM and MDM simulations respectively and assume  $\beta = 0.5$  for the Stromlo-APM data (see §4). The continuous, dashed and dot-dashed lines in Figure 3 are the best fit curves for the Gaussian,  $|w|^{3/2}$  and exponential models respectively. The best-fit values of  $\langle w^2 \rangle^{1/2}$  together with 95% confidence limits as estimated from likelihood ratios are given in Table 2.

For the survey data, we see that the exponential velocity distribution model gives a marginally better fit to the observations than the  $|w|^{3/2}$  or Gaussian distributions. There is no obvious trend of  $\langle w^2 \rangle^{1/2}$  with separation  $\sigma$ , the 95% confidence range for  $\langle w^2 \rangle^{1/2}$  is roughly 100–1100 km s<sup>-1</sup>, with a maximum likelihood value around 500 km s<sup>-1</sup>. Note that our survey does not provide a strong constraint on small scale peculiar velocities simply due to the sparse-sampling strategy we have employed. It would be interesting to compare  $f(w)$  for the morphological and luminosity-selected subsamples defined in Paper 2, but unfortunately, the shot-noise errors on  $\xi(\sigma, \pi)$  for these subsamples are too large to test for variation of  $\langle w^2 \rangle^{1/2}$  with galaxy type or luminosity.

For both sets of simulations, the exponential model provides the best fit for the smallest  $\sigma$  bin ( $\sigma < 2h^{-1}$ Mpc) but this model fails less well at larger projected separation. In fact none of the

models for  $f(w)$  provides a very good fit to the simulations, which probably explains why  $\langle w^2 \rangle^{1/2}$  is being overestimated for the simulations at small  $\sigma$ . (Using the position and velocity information for each galaxy in the simulations yields direct measurement of rms peculiar velocities of 350 km/s and 510 km/s for the LCDM and MDM model respectively.) Our fits to  $\langle w^2 \rangle^{1/2}$  in Table 2 are giving close to the expected values for  $\sigma \approx 5h^{-1}\text{Mpc}$ . We conclude that the LCDM model has slightly smaller peculiar velocities than the data, whereas peculiar velocities in the MDM model are comparable to those measured from the Stromlo-APM data.

### 3 Testing Estimators for $\beta$

In the preceding section we showed that the simulations have comparable two-point clustering statistics and small-scale peculiar velocities to the survey data. One might naively expect that if the simulations obey linear theory at a certain scale then linear theory should also be applicable to the survey data on that same scale. However, as seen below, we find that the MDM simulations show evidence for non-linear effects to much larger scales than the LCDM simulations, despite the relatively small difference in small-scale peculiar velocities. As pointed out by Fisher and Nusser (1996), the departure from linear theory is due to non-linear streaming (as modelled, for example, by the Zel'dovich approximation), and not just due to virialized motions.

In this section we investigate the scales on which linear theory is obeyed by the simulations, insofar as one can estimate  $\beta$  from the *anisotropy* of clustering in redshift space and from the *amplification* in  $\xi(s)$  in redshift space compared to real space.

#### 3.1 Anisotropy of $\xi(\sigma, \pi)$

We estimate the anisotropy in  $\xi(\sigma, \pi)$  as follows. The redshift space spherical harmonics  $\xi_l(r)$  in equation (4) are given by an integral over the full redshift space correlation function  $\xi(r, \mu)$ ,

$$\xi_l(r) = \frac{2l+1}{2} \int_{-1}^1 \xi(r, \mu) P_l(\mu) d\mu, \quad (13)$$

where  $P_l(\mu)$  is the  $l$ th order Legendre polynomial. We can measure  $\xi(r, \mu)$  by comparing the observed, weighted sum of galaxy pairs  $w_{dd}(r, \mu)$  at separation  $r$  and direction cosine to line of sight  $\mu$ , with the expected background  $\text{bgr}(r, \mu)$  for an isotropic, unclustered distribution. The line of sight direction is defined as the bisector in angle of each pair.

Since  $P_l(\mu)$  is an odd function for odd  $l$  and an even function for even  $l$ , the odd- $l$  harmonics vanish and the even- $l$  harmonics are given by

$$\begin{aligned} \xi_l(r) &= (2l+1) \int_0^1 \left( \frac{w_{gg}(r, \mu)}{\text{bgr}(r, \mu)} - 1 \right) P_l(\mu) d\mu \\ &\approx (2l+1) \Delta\mu \left[ \sum_{\text{pairs}(r)} \frac{w_i w_j P_l(\mu)}{\text{bgr}(r, \mu)} \right] - \delta_{l0}. \end{aligned} \quad (14)$$

Here we have replaced the integral over  $\xi(r, \mu)$  with respect to  $\mu$  by the weighted and appropriately normalised sum of  $P_l(\mu)$  for all galaxy pairs at separation  $r$ . The  $w_i w_j$  are the products of the

weights of each galaxy in the pair, given by equation (1) of Paper 2 and  $\delta_{l0}$  is the Kronecker delta symbol, equal to unity for  $l = 0$ , zero otherwise. The background  $\text{bgr}(r, \mu)$  is obtained by linear interpolation in  $\mu$  from a pre-calculated look-up table. We do not interpolate between  $r$ -bins, since the  $\xi_l(r)$  are calculated in the same separation bins in which  $\text{bgr}(r, \mu)$  is tabulated. This look-up table is generated in ten fixed steps in  $\Delta \log r$  and  $\Delta \mu$  using a large catalogue of random points with the same selection function and within the same boundaries as the data, and using the same weighting scheme,

$$\text{bgr}(r, \mu) = \frac{[w_{gr}(r, \mu)]^2}{w_{rr}(r, \mu)}. \quad (15)$$

Here  $w_{gr}(r, \mu)$  and  $w_{rr}(r, \mu)$  are the summed weights of galaxy-random and random-random pairs respectively. This definition of the background does not require one to estimate the mean density of the data and random catalogues to normalize  $\xi$ ; instead the normalisation is determined using only those galaxies at separation  $r$  and cosine direction  $\mu$ . Such an estimator gives more stable estimates of  $\xi$  on large scales than traditional estimators (Hamilton 1993b; Paper 2). In Figures 4a and b we plot the  $\xi_l(r)$  measured from the LCDM and MDM simulations respectively as the points with error bars. Also shown by the curves are the linear-theory predictions for the  $\xi_l(r)$  using equations (6)–(9) of Hamilton (1992).

For the LCDM model (Figure 4a), we use the power spectrum of Efstathiou, Bond and White (1992) with  $\Gamma = 0.2$  and  $\beta = 0.38$ . In this theory,  $\Gamma = \Omega_0 h$  determines the shape of the real-space correlation function, and  $\beta$  determines the redshift-space distortions. Since the simulations are unbiased,  $\beta = \Omega_0^{0.6} = 0.38$ . We see that the direction-averaged correlation function  $\xi_0$  measured from the simulations agrees well with linear theory on scales as small as  $2h^{-1}\text{Mpc}$ . Non-linearity is a far more severe problem for the quadrupole ( $\xi_2$ ) and hexadecapole ( $\xi_4$ ) harmonics. The quadrupole harmonic is expected to be negative in the linear regime (Hamilton 1992) and so we plot  $-\xi_2$  in Figure 4. The measured  $\xi_2$  is in fact positive on scales  $r \lesssim 15h^{-1}\text{Mpc}$  suggesting that non-linear effects dominate  $\xi_2$  on these scales. The amplitude of  $\xi_2$  is lower than that predicted by linear theory until  $r \approx 30h^{-1}\text{Mpc}$ , suggesting that non-linearity may affect  $\xi_2$  out to these scales. Beyond  $\sim 55h^{-1}\text{Mpc}$  the data is too noisy to measure  $\xi_2$  reliably. The hexadecapole harmonic  $\xi_4$  has an amplitude on scales  $r \lesssim 15h^{-1}\text{Mpc}$  exceeding the linear theory prediction by several orders of magnitude (in fact it is comparable to the direction-averaged correlation  $\xi_0$ ) and on larger scales, it's measurement is too noisy to be useful. Equation (4) gives physically reasonable estimates of the quantity  $\beta$  over a range of scales 21–42  $h^{-1}\text{Mpc}$ :  $\beta = 0.06 \pm 0.43$ ,  $0.47 \pm 0.48$  and  $0.02 \pm 0.35$  respectively at separations of  $r \approx 21, 30$  and  $42 h^{-1}\text{Mpc}$ . Comparison with the linear theory curves suggests that the first of these estimates (at  $r \approx 21h^{-1}\text{Mpc}$ ) is probably biased low by non-linearity, but the second two estimates appear to be in the linear regime.

For the MDM model (Figure 4b), we use the power spectrum of Klypin *et al.* (1993). Again, we see that the direction-averaged correlation function  $\xi_0$  agrees very well with linear theory over all scales measured but that  $\xi_2$  is only in reasonable agreement for scales  $r \gtrsim 15h^{-1}\text{Mpc}$ . The measured errors for  $\xi_4$  are very large on all scales, so we do not show the  $\xi_4$  estimates on this plot. At scales  $r \approx 21, 30$  and  $42 h^{-1}\text{Mpc}$ , equation (4) provides estimates of  $\beta$  of  $0.30 \pm 0.31$ ,  $0.39 \pm 0.44$  and  $0.61 \pm 0.86$ , all of which underestimate the true value  $\beta = 1$ .

### 3.2 Amplification of $\xi(s)$

We have seen in the previous subsection that *anisotropies* in the redshift space correlation function only agree with the linear theory prediction on very large scales, where measurements from existing galaxy catalogues are too noisy to usefully constrain  $\beta$ . In this subsection, we investigate how well one might measure  $\beta$  from the *amplification* of the direction-averaged correlation function in redshift space compared to real space.

The ratio  $\xi(s)/\xi(r)$  is subject to large random fluctuations in the linear regime where  $\xi(r)$  is small. Therefore, when estimating  $\beta$  from equation (5) it is desirable to either fit to  $\beta$  measured over a range of scales or alternatively to smooth the  $\xi$  estimates before taking their ratio. A common way of smoothing  $\xi(r)$  is to take its volume integral

$$J_3(r) = \int_0^r x^2 \xi(x) dx. \quad (16)$$

With an  $N$ -body simulation, one has the advantage of being able to estimate the real space correlation function directly by using the real space locations of the simulation galaxies in (6), as well as via inversion of the projected correlation function (7). The former estimate of  $\xi(r)$  is useful for studying effects of non-linearity in the simulations, whereas the latter, noisier, estimate gives a more realistic assessment of what we can hope to measure from real data. We have used the ratios  $\xi(s)/\xi(r)$  and  $J_3(s)/J_3(r)$  measured with both  $\xi(r)$  estimates in equation (5) to estimate  $\beta$  on a range of scales. These estimates are presented in Figures 5 and 6 for the LCDM and MDM simulations respectively.

For the LCDM simulations (Fig. 5), we see that the ratio  $\xi(s)/\xi(r)$  (open symbols) appears to converge to give the correct value of  $\beta$  by a scale  $r \approx 5h^{-1}\text{Mpc}$ , although the estimates are biased a little high. Beyond  $r \approx 20h^{-1}\text{Mpc}$ , the measured correlation functions are too noisy to usefully constrain  $\beta$ . We have calculated a maximum-likelihood fit to the four data points between 5 and 16  $h^{-1}\text{Mpc}$ , and find that  $\beta = 0.56$  with a 95% confidence range 0.44–0.68. The ratio  $J_3(s)/J_3(r)$  (solid symbols) is biased low by non-linear dynamics to larger scales ( $r \approx 20h^{-1}\text{Mpc}$ ), but by these scales is providing an almost unbiased and low-noise estimate of the true  $\beta$ . The point at  $r = 17.8h^{-1}\text{Mpc}$  yields  $\beta = 0.29 \pm 0.07$  (one sigma error). The results using  $\xi(r)$  and  $J_3(r)$  inferred from inversion of the projected correlation function (Fig. 5b) are only a little noisier than those determined from the direct estimates of  $\xi(r)$  and  $J_3(r)$ . Fitting to  $\beta_\xi$  over the same four measurements provides  $\beta = 0.58$  with a 95% confidence limit 0.41–0.76 and  $\beta_{J_3}(17.8) = 0.36 \pm 0.13$ .

For the MDM simulations (Fig. 6), we see that the ratio  $\xi(s)/\xi(r)$  (open symbols) does not converge so readily to the correct value of  $\beta$ ; it crosses  $\beta = 1$  at  $r \approx 10h^{-1}\text{Mpc}$  but then tends to overshoot slightly. Again, beyond  $r \approx 20h^{-1}\text{Mpc}$ , the measured correlation functions are too noisy to usefully constrain  $\beta$ . A fit to  $\beta_\xi$  using the two measurements in the range 10–16  $h^{-1}\text{Mpc}$  provides the estimates  $\beta = 1.41$  (1.00–1.83) and  $\beta = 0.93$  (0.72–1.15) for the direct and inverted estimates of  $\xi(r)$  respectively. The ratio  $J_3(s)/J_3(r)$  (solid symbols) converges to  $\beta = 1$  by scales  $r \approx 20h^{-1}\text{Mpc}$ ; estimates on larger scales tend to overestimate  $\beta$ , but most are within  $\sim 1\sigma$  of  $\beta = 1$ . We measure  $\beta_{J_3}(17.8) = 1.02 \pm 0.16$  and  $\beta_{J_3}(17.8) = 0.85 \pm 0.17$  from Figs. 6 (a) and (b) respectively.

One could consider using alternative, smoothed measures of the galaxy clustering which are less affected by small-scale peculiar velocities than  $J_3$ . An example would be a modified form of the  $J_3$  integral in which the lower limit of integration is set at, say,  $r_{\min} = 5h^{-1}\text{Mpc}$ . This was tried,

and while the contribution from peculiar velocities is indeed suppressed, the modified estimator is subject to larger random fluctuations than  $J_3$  as defined in (16).

### 3.3 Conclusions from Simulations

We have analysed two ensembles of CDM-like  $N$ -body simulations, one a low density (LCDM,  $\Omega_0 = 0.2$ ) model, and one high density (MDM,  $\Omega_0 = 1$ ). Both give a reasonable match to the real and redshift space correlation functions measured from the Stromlo-APM Redshift Survey and have comparable peculiar velocities  $\langle w^2 \rangle^{1/2}$ . We used these simulations to investigate the practicality of measuring the quantity  $\beta = \Omega_o^{0.6}/b$  from (a) the anisotropy and (b) the amplification of the measured galaxy clustering in redshift space.

For the LCDM simulations, we find that the 2nd and 4th order spherical harmonics of the redshift space correlation function are severely affected by non-linearities to scales  $r \sim 30h^{-1}\text{Mpc}$ , and so one needs a reliable measurement of the  $\xi_l$  on scales  $r \gtrsim 30h^{-1}\text{Mpc}$  in order for linear theory to be applicable. This is in agreement with the Fourier-space harmonic analysis of Cole *et al.* (1994). The situation is even worse for the MDM simulations, where the 2nd order spherical harmonic underestimates  $\beta$  on *all* scales at which it can be measured reliably.

By contrast, the amplitude of the direction averaged correlation function  $\xi_0$  is relatively weakly affected by non-linearity. For the LCDM model non-linear effects become unimportant on much smaller scales,  $r \sim 5h^{-1}\text{Mpc}$  for  $\xi$  measures and  $r \sim 20h^{-1}\text{Mpc}$  for  $J_3$  measures. The MDM simulations effectively agree with linear theory by scales of  $r \approx 10h^{-1}\text{Mpc}$  for the  $\xi$  measures and by  $r \approx 20h^{-1}\text{Mpc}$  for the  $J_3$  measures.

Thus the more practical method for determining  $\beta$  from current redshift surveys is by comparison of the direction-averaged redshift-space correlation function with the real-space correlation function. By using the  $J_3$  volume integral over  $\xi$ , one decreases the random noise in  $\beta$ , at the expense of pushing out the effects of non-linearity to larger scales. In practice it will be worthwhile to estimate  $\beta$  from both  $\xi(s)/\xi(r)$  and  $J_3(s)/J_3(r)$ . We expect the  $J_3$  ratio to give the less noisy results.

## 4 Results from Stromlo-APM Survey

### 4.1 Constraints on $\beta$

We have measured the spherical harmonics  $\xi_l(s)$  of the Stromlo-APM redshift space correlation function in the same way as for the simulations (§3.1). The results are shown as the points with error bars in Figure 7. The curves show the linear theory predictions for LCDM (light lines) and MDM (heavy lines). We see pronounced effects of non-linearity and very large error bars on the  $\xi_2$  harmonics on scales smaller than  $20h^{-1}\text{Mpc}$ . The direction-averaged correlation function  $\xi_0$  is well matched by the LCDM linear theory prediction on all scales. The MDM model slightly under-predicts  $\xi_0$  on small and large scales (cf Fig. 2). The measured  $\xi_2$  harmonics agree quite well with the LCDM linear theory prediction on scales 20–50  $h^{-1}\text{Mpc}$  whereas the MDM prediction is too high. In other words, we see evidence for smaller redshift space distortions than expected in an unbiased  $\Omega_0 = 1$  model. On scales of 21, 30 and 42  $h^{-1}\text{Mpc}$ , the estimated values of  $\beta$  are  $0.41 \pm 0.17$ ,  $-0.03 \pm 0.29$  and  $0.23 \pm 0.31$  respectively.

From our analysis of simulated galaxy catalogues in the previous section, we expect the ratios of the direction-averaged clustering in redshift space and real space to give more reliable estimates of  $\beta$ . In Figure 8, we plot our estimates of  $\beta$  from the redshift survey, as determined from the ratio  $\xi(s)/\xi(r)$  (open symbols) and from the ratio  $J_3(s)/J_3(r)$  (solid symbols). The error bars in this figure are determined from the scatter between estimates of  $\beta$  for each of the nine bootstrap resampled surveys, and are in reasonable agreement with the scatter found between different realizations of the simulations (Figs. 5 and 6) in the linear regime. There is a wide scatter in the  $\beta$  estimates from the  $\xi$  ratios around 10–20  $h^{-1}$ Mpc, but the  $J_3$  ratios give consistent results over this range, appearing to favour  $\beta \approx 0.2$ –0.5. Even the point giving the largest value of  $\beta$  ( $\beta = 0.48 \pm 0.12$  at  $r = 17.8h^{-1}$ Mpc) favours  $\beta \ll 1$ . It is interesting to note that in both sets of simulations, the  $J_3$  ratio at this scale provides an estimate of  $\beta$  within 1 sigma of the correct value. Therefore  $\beta \lesssim 0.6$  would seem to be a reasonable upper limit allowed by our analysis and we conclude that either  $\Omega_0 < 1$  or that galaxies are significantly biased tracers of the mass distribution,  $b \gtrsim 2$ .

As an aside, we note that the small-scale, non-linear, behaviour of  $\beta$  for the Stromlo-APM survey is markedly different to that of the simulations, which have a systematically negative  $\beta$  and smaller errors on scales  $r \lesssim 5h^{-1}$ Mpc. We are not overly concerned by this as the simulations provide a relatively poor fit to observed clustering on small scales and we know that equation (5) is clearly not to be trusted in regimes in which it predicts a negative  $\beta$ !

## 4.2 Disentangling $\Omega$ and $b$

Ideally, of course, one would like to know the values of the density parameter  $\Omega$  and the bias parameter  $b$  individually. Cole *et al.* (1994) have discussed how it may be possible with future redshift surveys to separate the determination of  $\Omega$  and  $b$  by studying the scaling of non-linear effects. An alternative approach is the study of high order correlations to constrain the (possibly non-linear) biasing model using weakly non-linear perturbation theory. Gaztañaga and Frieman (1994) have used high order moments of APM galaxies to constrain biasing models. To be consistent with non-linear perturbation theory, one should allow the possibility of *non-linear* bias, in which case second- and third-order non-linear bias coefficients can be chosen which match the observed high order correlations. However, the observations are very well fit by an *unbiased*, low-density CDM model with  $b \approx 1$ . Applying Occam’s razor, this seems the more natural solution.

## 4.3 Relative Biasing of Different Galaxy Types

Despite the uncertainties in the value of galaxy bias with respect to the mass, one may study the *relative* bias of galaxies of different type by comparing their clustering properties. There are two independent ways to measure the relative bias factors: (1) by comparing real-space clustering in the linear regime and (2) by measuring the redshift space amplification of clustering due to equation (5). One thus has a consistency check on measurements of  $\beta$  and relative bias parameters. We have already compared the clustering of galaxies of different luminosity and morphological type in Paper 2. In that paper we concentrated on the small-scale (power-law) regime of galaxy clustering. Here we study clustering in the linear regime. We analyse galaxy subsamples from the Stromlo-APM survey of low, middle and high luminosity, and of early and late type. These galaxy samples are defined in Table 1 of Paper 2.

In Figure 9 we plot the relative bias values  $b_\xi = \xi_{tg}(r)/\xi_{gg}(r)$  (open symbols) and  $b_{J_3} = J_3^{tg}(r)/J_3^{gg}(r)$  (solid symbols) for each sample over a range of scales. We have divided the real-space cross-correlation of each sample with the parent APM galaxy sample (Paper 2) by the real-space cross-correlation function of the ‘all galaxies’ sample, hence the relative bias for the ‘all galaxies’ sample is defined to be unity. The error bars are determined from the one sigma scatter in  $b_\xi$  from the nine bootstrap-resampled versions of the survey data. Given that our estimates of  $\xi(r)$  are unreliable beyond  $r \approx 20h^{-1}\text{Mpc}$ , we see no obvious trend of relative bias with scale in the linear regime. We have therefore calculated the maximum-likelihood value of  $b_\xi$  over the range 5–12  $h^{-1}\text{Mpc}$ , a regime over which the assumption of linear bias seems reasonable and where our measurement errors are not too large. These values, along with the 95% confidence limits, are given in Table 3. We also show the relative bias  $b_{J_3}$  measured at a separation of  $r = 17.8h^{-1}\text{Mpc}$  in this table. We see that low-luminosity galaxies (sample b), are only about one third as strongly clustered as middle-luminosity galaxies, in accordance with the findings of Paper 2. High luminosity galaxies (sample d) appear to be about thirty percent more strongly clustered than middle-luminosity galaxies, although the 95% confidence limits do allow for no difference in clustering, again in accord with Paper 2. Early type galaxies (e) have a very similar bias parameter to luminous galaxies, whereas late type galaxies have a bias parameter midway between that of low and middle-luminosity galaxies.

The parameter most commonly used for normalizing the power spectrum of clustering models and theories to observations is the variance of galaxy counts in  $8h^{-1}\text{Mpc}$  radius spheres,  $(\sigma_8^2)_g$ ,

$$(\sigma_8^2)_g = \frac{1}{V^2} \int \int_V \xi(r_{12}) dV_1 dV_2. \quad (17)$$

We estimate  $(\sigma_8^2)_g$  by Monte-Carlo integration of the observed real-space correlation function for each of the galaxy samples using 500,000 randomly placed pairs of points inside an  $8h^{-1}\text{Mpc}$  radius sphere. Results are given in Table 3. As we see from Figures 5 and 6,  $(\sigma_8^2)_g$  may be mildly affected by non-linearity, and so we do not expect  $b_\xi$  and  $b_{J_3}$  to be directly proportional to  $(\sigma_8)_g$ . Note the significant difference in  $(\sigma_8^2)_g$  for galaxies fainter than  $L^*$  and those around  $L^*$  and brighter.

In Figure 10 we plot estimates of  $\beta_\xi$  (open symbols) and  $\beta_{J_3}$  (solid symbols) for each galaxy sample. In order to estimate  $\beta$  for galaxy sub-samples, we have measured the redshift-space cross-correlation function of the given galaxy sample with the all-galaxies sample using the estimator

$$1 + \xi_{tg}(s) = \frac{w_{tg}(s)w_{rr}(s)}{w_{tr}(s)w_{gr}(s)}. \quad (18)$$

Here the subscript  $t$  denotes galaxies of specific type,  $g$  denotes all galaxies and  $r$  denotes random points (cf. eq. 6). Comparing this with the real-space cross correlation function  $\xi_{tg}(r)$  gives an estimate of  $\beta$  via equation (5). Once again, the error bars come from the scatter between bootstrap resamplings. Estimates of  $\beta_\xi$  and 95% confidence limits over the separation range 5–12  $h^{-1}\text{Mpc}$  are given in Table 3. Clearly, negative values or lower limits on  $\beta$  are not physically reasonable, but the upper limits are still useful. For instance, for bright galaxies (d) we can say that  $\beta < 0.9$  with 95% confidence. The value of  $\beta_{J_3}$  at  $r \approx 17.8h^{-1}\text{Mpc}$  is also given in Table 3.

Now, if the ‘true’ bias factor  $b_t^{\text{true}}$  (ie. the bias with respect to the mass) is related to the relative bias factor by  $b_t^{\text{true}} = b_0 b_t$ , (so that  $b_0$  is the bias factor for the ‘all galaxies’ sample) then the product  $b_t \beta$  for each galaxy sample should be a constant equal to  $\Omega^{0.6}/b_0$ . While we do find some scatter in this quantity between the different samples, the results are consistent ( $\Omega^{0.6}/b_0 \approx 0.2\text{--}0.6$ ) within the 95% confidence limits.

## 5 Conclusions

We have used large and realistic  $N$ -body simulations to investigate the effects of non-linearity on two estimators for the quantity  $\beta$  (eqs. [4] and [5]) in low and high density models. We find that non-linearity affects the 2nd order spherical harmonic  $\xi_2(s)$  of redshift space clustering to scales as large as  $30h^{-1}\text{Mpc}$ . In contrast, the amplitude of the direction-averaged correlation function  $\xi_0(s)$  is only weakly affected by non-linearity on scales  $r \gtrsim 5h^{-1}\text{Mpc}$  in the LCDM model and  $r \gtrsim 10h^{-1}\text{Mpc}$  in the MDM model. Therefore the most practical method for constraining  $\beta$  with existing redshift surveys is by measuring the amplification of direction-averaged redshift space clustering over real space clustering. An alternative approach, modeling the non-linearity, has recently been used by Cole *et al.* (1995) and Fisher and Nusser (1996). These authors also find that  $\beta \lesssim 0.6$  from independent data sets.

Measuring the projected cross-correlation of Stromlo-APM galaxies with the parent APM survey galaxies enables a reliable determination of  $\xi(r)$  to scales  $r \lesssim 20h^{-1}\text{Mpc}$ . The ratio  $\xi(s)/\xi(r)$  shows rather large scatter on scales  $5\text{--}20 h^{-1}\text{Mpc}$ , but the integral  $J_3$  is less noisy than  $\xi(r)$  and on a scale  $r \approx 17.8h^{-1}\text{Mpc}$ ,  $J_3(s)/J_3(r)$  provides the estimate  $\beta = 0.48 \pm 0.12$ . A reasonable upper limit on  $\beta$  from this analysis is  $\beta \lesssim 0.6$ . Given that the  $\beta_{J_3}$  estimates on either side of  $r \approx 17.8h^{-1}\text{Mpc}$  are almost consistent with  $\beta = 0$ , we regard our analysis as providing an *upper limit* of  $\beta \lesssim 0.6$ , rather than an actual estimate of  $\beta$ . Although a little lower than estimates of  $\beta$  from peculiar velocity analyses (eg. Hudson *et al.* 1995, who find  $\beta = 0.74 \pm 0.13$ ), the largely unknown systematic errors in most current estimates of  $\beta$  means they are all fairly consistent. See Dekel (1994) or Strauss and Willick (1995) for a review of recent measurements of  $\beta$ .

The Stromlo-APM survey is a powerful sample for constraining  $\beta$  since the large volume probed enables us to reliably measure redshift space galaxy clustering in the linear regime, whereas many previous analyses have been limited to measuring  $\xi(s)$  in the non-linear regime. Cross-correlation with the fully-sampled APM galaxy survey enables us to measure  $\xi(r)$  much more accurately than using the angular correlation function  $w(\theta)$ , and thus the technique of using the ratio  $\xi(s)/\xi(r)$  [or  $J_3(s)/J_3(r)$ ] comes into its own for this survey. The most likely source of systematic error in this analysis is in the inversion of the projected correlation function  $\Xi(\sigma)$  to obtain the real space correlation function  $\xi(r)$ . Comparison of the  $\beta$  determinations from the simulations using  $\xi(r)$  measured directly from the simulations and via inversion of the projected correlation function (§3.2) suggests that any such error is comparable to or smaller than random errors.

With linear theory and 2-point clustering statistics alone one cannot separate the contributions of  $\Omega$  and  $b$  in  $\beta = \Omega^0.6/b$ . However, as Gaztañaga and Frieman (1994) have discussed, higher order correlations may be used to constrain biasing models. Their analysis of APM galaxies favours a linear bias parameter  $b \approx 1$ , although to be strictly self-consistent, one should allow for a non-linear bias model in non-linear perturbation theory, in which case one can always match the observed skewness of APM galaxy counts in cells by adjusting the non-linear bias parameters. Further work is clearly required in constraining possible biasing models.

As we have seen in Paper 2, different classes of galaxy have different clustering properties, and so not all galaxies can have exactly the same biasing parameter. In particular, low-luminosity galaxies are about three times less strongly clustered than  $L^*$  galaxies on large scales, and so  $b_{L^*} \approx 3b_{<L^*}$ . An interesting test would be to see if high order clustering of low-luminosity galaxies also predicts a lower value of bias than for  $L^*$  galaxies.

In conclusion, we find that a relatively low value of  $\beta$  is favoured by the Stromlo-APM data; our results appear to rule out an unbiased,  $\Omega = 1$  model. We thus conclude that  $\Omega < 1$  and/or that galaxies are positively biased, ie. more strongly clustered than the underlying mass distribution.

Acknowledgments: we are indebted to Andrew Hamilton for invaluable e-mail correspondence and to Peter Quinn for useful discussions during the early stages of this project. We thank Albert Stebbins for pointing out an error in an earlier version of this paper and the anonymous referee who suggested that we test our methods on a high-density simulation. JL acknowledges the hospitality of the Oxford Physics Department where the final version of this paper was completed.

## Tables

Table 1: Power-law fits to real and redshift space clustering in the survey data and simulations.

Sample	$\gamma_s$	$s_0$	$\gamma_r$	$r_0$
Stromlo – APM	$1.49 \pm 0.15$	$5.9 \pm 0.4$	$1.71 \pm 0.05$	$5.1 \pm 0.2$
LCDM	$1.84 \pm 0.16$	$6.1 \pm 0.5$	$1.97 \pm 0.12$	$6.0 \pm 0.6$
MDM	$1.37 \pm 0.15$	$4.3 \pm 0.2$	$1.48 \pm 0.09$	$3.9 \pm 0.9$

Notes.— $\gamma_s$  and  $s_0$  are the power-law fit parameters to the correlation function in redshift space measured over the range 1.5–30  $h^{-1}$ Mpc.  $\gamma_r$  and  $r_0$  are the real-space power-law parameters over the range 0.2–20  $h^{-1}$ Mpc.

Table 2: Constraints on galaxy peculiar velocities (km s $^{-1}$ ) for survey data and simulations.

Model	Gaussian				$ w ^{3/2}$				Exponential			
	$\sigma$	$\langle w^2 \rangle^{1/2}$	95% conf	$\ln(\mathcal{L})$	$\langle w^2 \rangle^{1/2}$	95% conf	$\ln(\mathcal{L})$	$\langle w^2 \rangle^{1/2}$	95% conf	$\ln(\mathcal{L})$		
Survey Data												
1.0	383	89	756	−10.1	404	96	841	−9.9	438	101	1095	−9.9
3.0	400	203	800	−3.1	446	219	889	−2.9	531	253	1081	−2.6
5.0	406	98	832	−3.0	417	105	907	−2.9	459	112	1093	−2.9
7.0	271	0	708	0.0	271	0	796	0.0	282	0	1040	−0.1
LCDM Simulation												
1.0	473	443	504	−32.8	500	461	538	−20.7	569	519	631	−11.6
3.0	452	388	524	2.8	475	405	554	2.3	533	447	634	−0.2
5.0	228	153	299	7.5	234	155	311	7.4	247	158	336	7.1
7.0	283	185	380	10.6	293	187	396	10.5	310	191	432	10.2
MDM Simulation												
1.0	628	560	726	−0.5	698	610	788	3.6	847	743	975	5.3
3.0	480	425	543	10.3	513	453	585	10.5	601	521	690	8.0
5.0	472	395	566	8.2	498	409	601	7.2	552	448	691	4.9
7.0	396	302	497	0.3	404	305	515	−0.7	430	313	560	−2.8

Table 3: Relative bias  $b_\xi$  and  $b_{J_3}$ , variance in  $8h^{-1}\text{Mpc}$  cells  $(\sigma_8^2)_g$ , and redshift space distortion factors  $\beta_\xi$  and  $\beta_{J_3}$  for galaxy subsamples

Type	$b_\xi$	95% conf		$b_{J_3}$	$(\sigma_8^2)_g$	$\beta_\xi$	95% conf		$\beta_{J_3}$
<i>a</i> All	1.00	1.00	1.00	$1.00 \pm 0.00$	$0.89 \pm 0.05$	0.36	-0.03	0.75	$0.48 \pm 0.12$
<i>b</i> Faint	0.31	0.05	0.56	$0.32 \pm 0.18$	$0.40 \pm 0.10$	1.91	0.35	3.46	$0.85 \pm 0.71$
<i>c</i> Middle	1.05	0.85	1.26	$1.15 \pm 0.13$	$1.08 \pm 0.14$	0.26	-0.12	0.65	$0.59 \pm 0.29$
<i>d</i> Bright	1.34	0.78	1.89	$1.45 \pm 0.35$	$1.20 \pm 0.18$	-0.11	-1.14	0.91	$0.19 \pm 0.43$
<i>e</i> E&S0	1.39	0.83	1.95	$1.36 \pm 0.35$	$1.24 \pm 0.27$	0.44	-0.13	0.99	$0.27 \pm 0.59$
<i>f</i> Sp&Irr	0.78	0.62	0.95	$0.87 \pm 0.12$	$0.66 \pm 0.05$	0.30	-0.16	0.75	$0.33 \pm 0.45$

## REFERENCES

- Barrow, J.D., Bhavsar, S.P. and Sonoda, D.M., 1984, MNRAS, 210, 19p
- Bean, A.J., Efstathiou, G., Ellis, R.S., Peterson, B.A. and Shanks, T., 1983, MNRAS, 205, 605
- Cole, S., Fisher, K.B. and Weinberg, D.H., 1994, MNRAS, 267, 785
- Cole, S., Fisher, K.B. and Weinberg, D.H., 1995, MNRAS, 275, 515
- Croft, R.A.C. and Efstathiou, G., 1994, MNRAS, 268, L23
- Davis, M. and Peebles, P.J.E., 1983, ApJ, 267, 465
- Dekel, A., 1994, ARA&A, 32, 371
- Efstathiou, G., Bond, J.R. and White, S.D.M., 1992, MNRAS, 258, 1p
- Efstathiou, G., Ellis, R.S. and Peterson, B.A., 1988, MNRAS, 232, 431 (EEP)
- Fisher, K.B., Davis, M., Strauss, M.A., Yahil, A. and Huchra, J.P., 1994a, MNRAS, 267, 927
- Fisher, K.B. and Nusser, A., 1996, MNRAS, in press
- Fisher, K.B., Scharf, C.A. and Lahav, O., 1994b, MNRAS, 266, 219
- Gaztañaga, E. and Frieman, J.A., 1994, ApJ, 437, L13
- Hamilton, A.J.S., 1992, ApJ, 385, L5
- Hamilton, A.J.S., 1993a, ApJ, 406, L47
- Hamilton, A.J.S., 1993b, ApJ, 417, 19
- Heavens, A.F. and Taylor, A.N., 1995, MNRAS, 275, 483
- Hudson, M., Dekel, A., Courteau, S., Faber, S.M. and Willick, J.A., 1995, MNRAS, 274, 305
- Kaiser, N., 1987, MNRAS, 227, 1
- Loveday, J., Efstathiou, G., Peterson, B.A. and Maddox, S.J., 1992a, ApJ, 400, L43
- Loveday, J., Peterson, B.A., Efstathiou, G. and Maddox, S.J., 1992b, ApJ, 390, 338 (Paper 1)
- Loveday, J., Maddox, S.J., Efstathiou, G., and Peterson, B.A., 1995, ApJ, 442, 457 (Paper 2)
- Loveday, J., Peterson, B.A., Maddox, S.J. and Efstathiou, G., 1996, submitted to ApJ
- Maddox, S.J., Sutherland, W.J. Efstathiou, G., and Loveday, J., 1990a, MNRAS, 243, 692
- Maddox, S.J., Efstathiou, G. and Sutherland, W.J., 1990b, MNRAS, 246, 433
- Saunders, W., Rowan-Robinson, M. and Lawrence, A., 1992, MNRAS, 258, 134
- Strauss, M.A. and Willick, J.A., 1995, Phys. Rep., 261, 271
- Tadros, H., and Efstathiou, G., 1996, in preparation

## Figure Captions

**Figure 1** A contour plot of the full redshift space correlation function  $\xi(\sigma, \pi)$  measured from the Stromlo-APM Redshift Survey as a function of separation parallel ( $\pi$ ) and perpendicular ( $\sigma$ ) to the line of sight and smoothed with a  $\begin{Bmatrix} 1 & 2 & 1 \\ 2 & 4 & 2 \\ 1 & 2 & 1 \end{Bmatrix}$  smoothing filter. The contours are plotted in fixed steps in  $\log \xi$  from  $-3$  to  $1$ . Solid contours show values  $\xi \geq 1$ , dashed contours show values  $\xi < 1$  (*i.e.* in the linear regime).

**Figure 2** Comparison of the Stromlo-APM (filled circles), LCDM (open circles) and MDM (open squares) correlation functions in (a) redshift space and (b) in real space.

**Figure 3** The redshift-space correlation function  $\xi(\sigma, \pi)$  plotted as a function of separation  $\pi$  along the line of sight for four bins in projected separation  $\sigma$ . The points with error bars show  $\xi(\sigma, \pi)$  calculated from (a) the Stromlo-APM survey, (b) the LCDM simulation and (c) the MDM simulation. The curves show predictions for three peculiar velocity distribution functions — see text for details.

**Figure 4** (a) The First three spherical harmonics for the redshift-space correlation function measured from the LCDM simulations (symbols) and predicted by linear CDM theory (curves). Filled circles and the continuous line shows the direction-averaged correlation function ( $\xi_0$ ). Star symbols and the dashed line show the negative of the quadrupole harmonic ( $-\xi_2$ ). Open circles and the dotted line show the hexadecapole harmonic ( $\xi_4$ ). (b) As (a) for the MDM simulations.  $\xi_4$  is very noisy for this set of simulations and so is not shown here.

**Figure 5** Estimates of  $\beta$  as a function of separation from the LCDM simulations using equation (5), (a) uses ‘direct’ estimation of  $\xi(s)$  and  $\xi(r)$ , (b) uses the projected cross-correlation estimate of  $\xi(r)$  (Eq. 7). The open symbols show  $\beta$  estimated from the ratio  $\xi(s)/\xi(r)$  and the solid symbols show  $\beta$  estimated from the ratio  $J_3(s)/J_3(r)$ . The horizontal unbroken line shows the maximum-likelihood fit to  $\beta_\xi$  over the range indicated and the dotted lines show 95% confidence limits on this  $\beta$  estimate. The horizontal dashed line indicates the actual  $\beta = 0.38$  for these simulations.

**Figure 6** As Figure 5 but for the MDM simulations.

**Figure 7** The 0th and 2nd order spherical harmonics of the redshift-space correlation function measured from the Stromlo-APM survey. The curves are from LCDM linear theory (light lines) and MDM theory (heavy lines).

**Figure 8** Estimates of  $\beta$  as a function of separation for the Stromlo-APM survey data from the ratio  $\xi(s)/\xi(r)$  (open circles) and  $J_3(s)/J_3(r)$  (filled circles).

**Figure 9** Relative bias factors for subsamples of the Stromlo-APM Survey, determined from the ratio  $\xi_{tg}(r)/\xi_{gg}(r)$  (open circles) and  $J_3^{tg}(r)/J_3^{gg}(r)$  (filled circles). The horizontal lines show the maximum likelihood fit to  $\xi_{tg}(r)/\xi_{gg}(r)$  over the range 5–12  $h^{-1}\text{Mpc}$ ; the dashed lines show the 95% confidence limits.

**Figure 10** Estimates of  $\beta$  for subsamples of the Stromlo-APM Survey, determined from the ratio  $\xi_{tg}(s)/\xi_{tg}(r)$  (open circles) and  $J_3^{tg}(s)/J_3^{tg}(r)$  (filled circles).

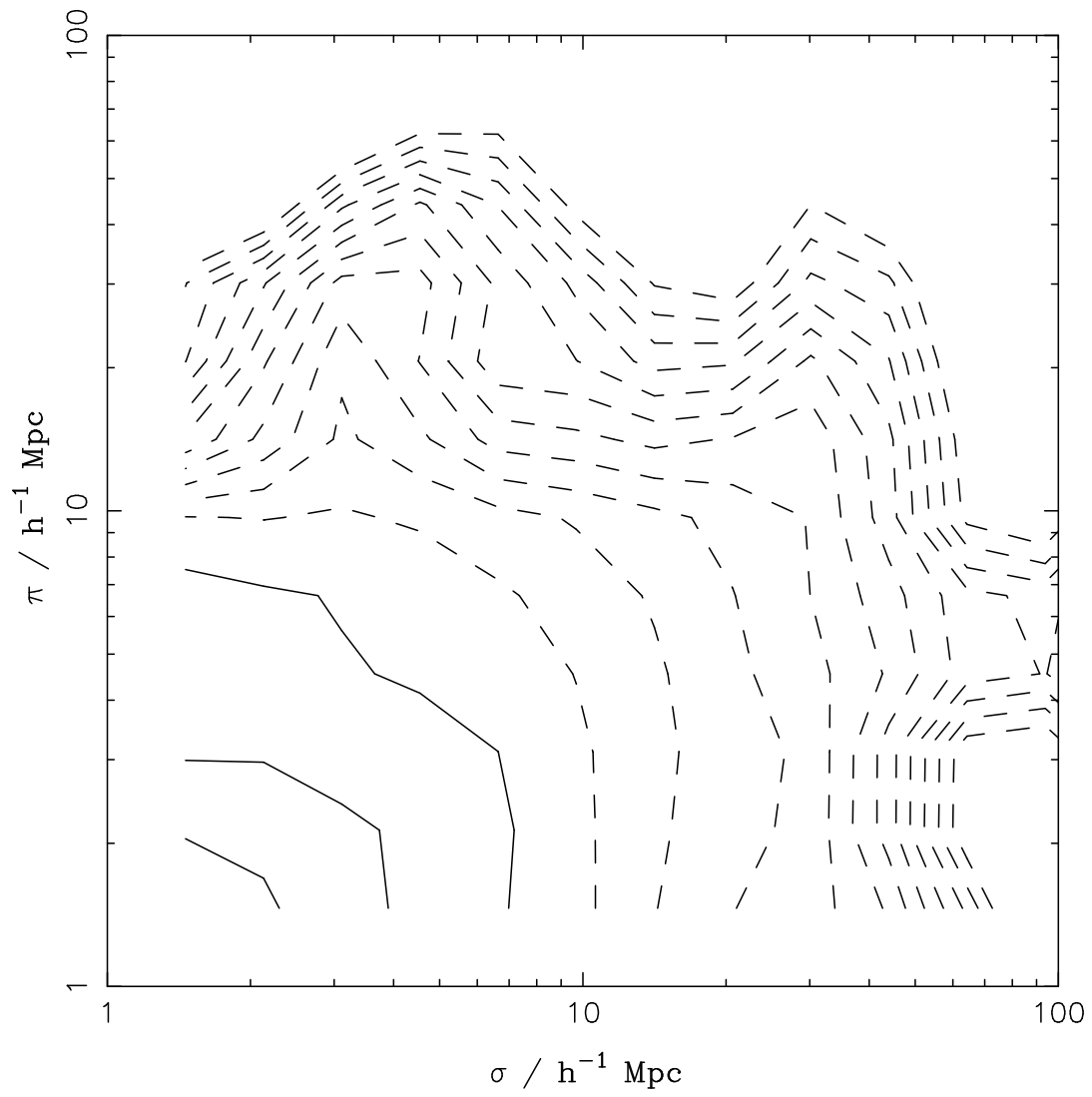


Figure 1:

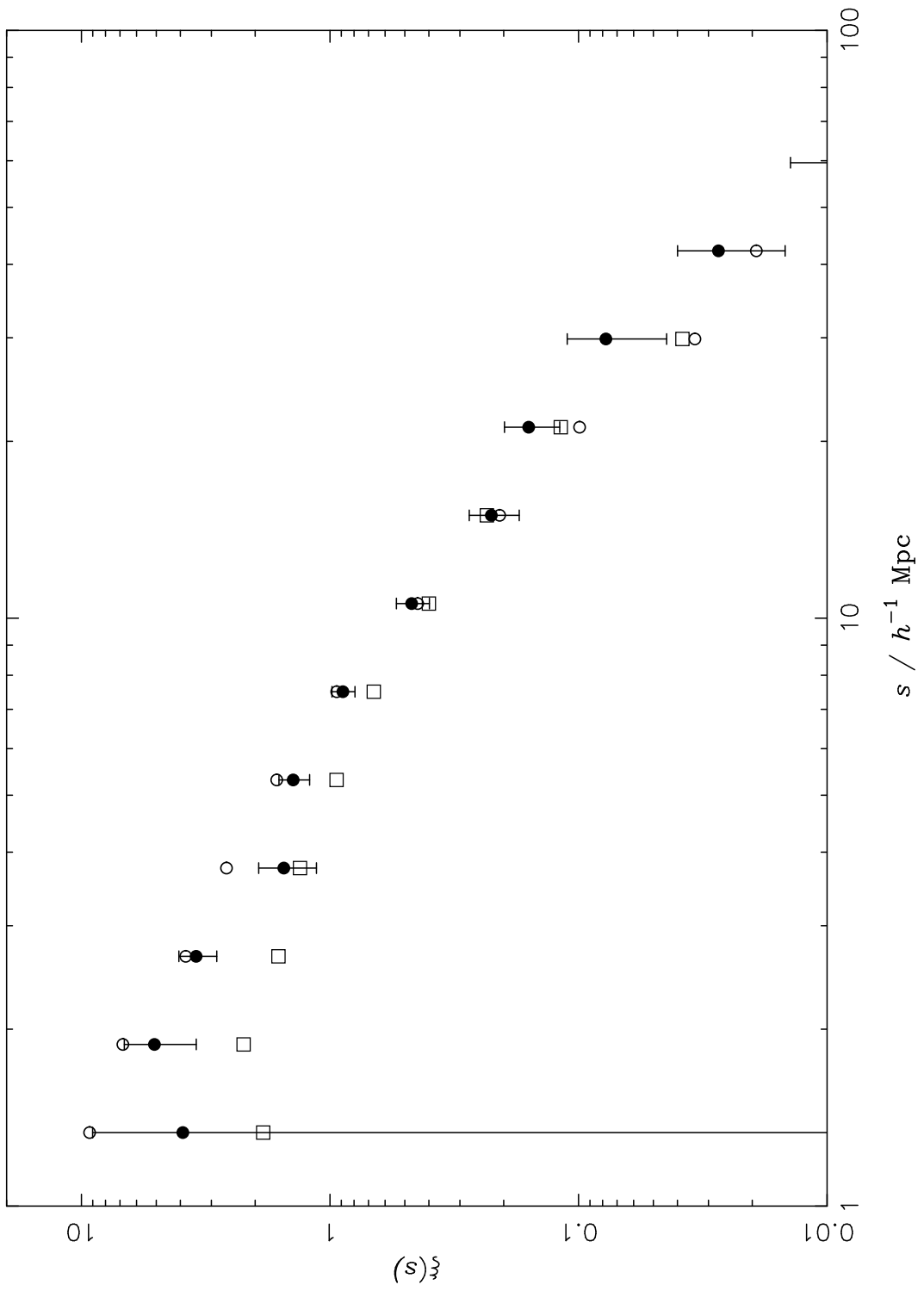


Figure 2: a

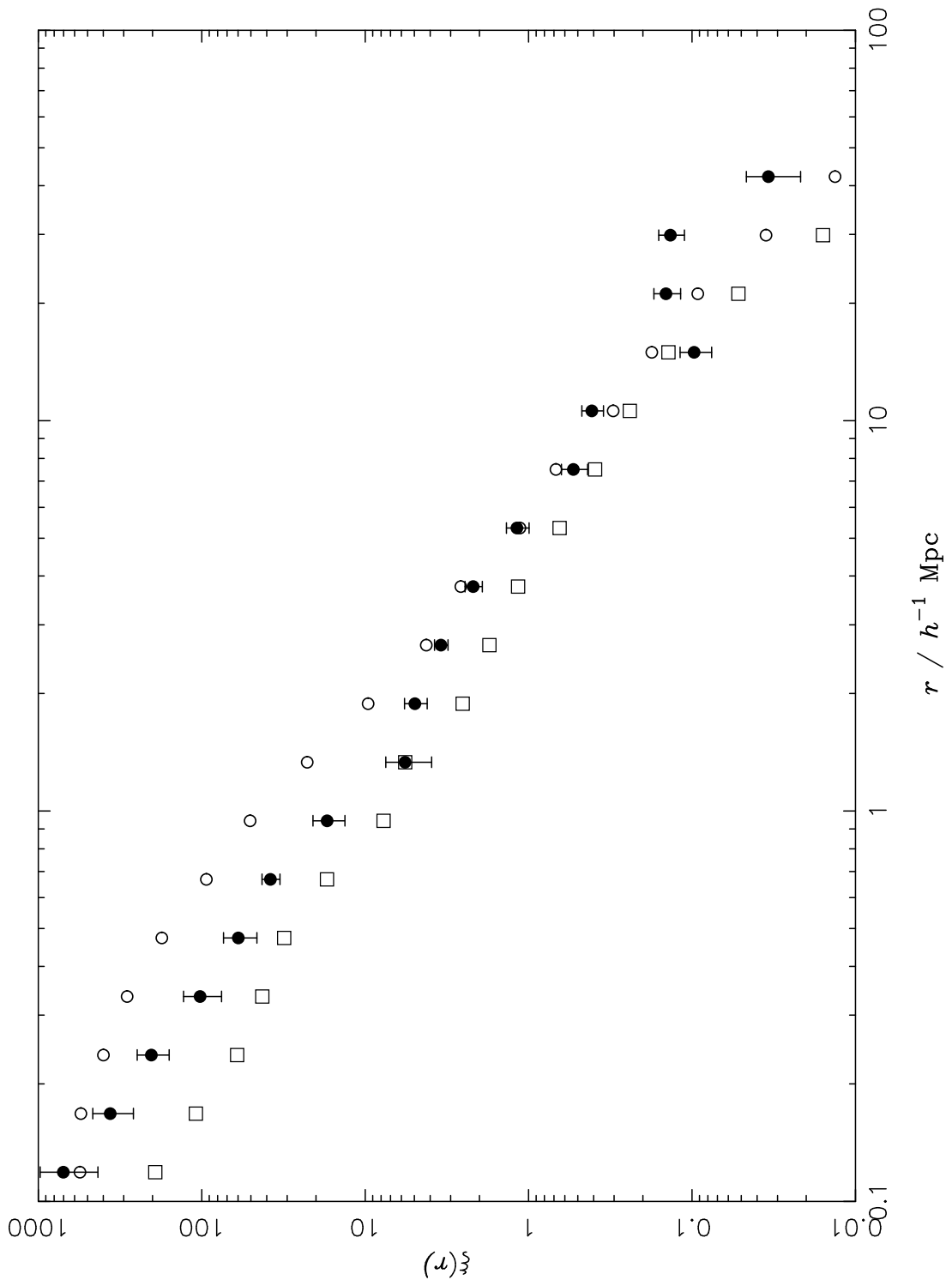


Figure 2: b

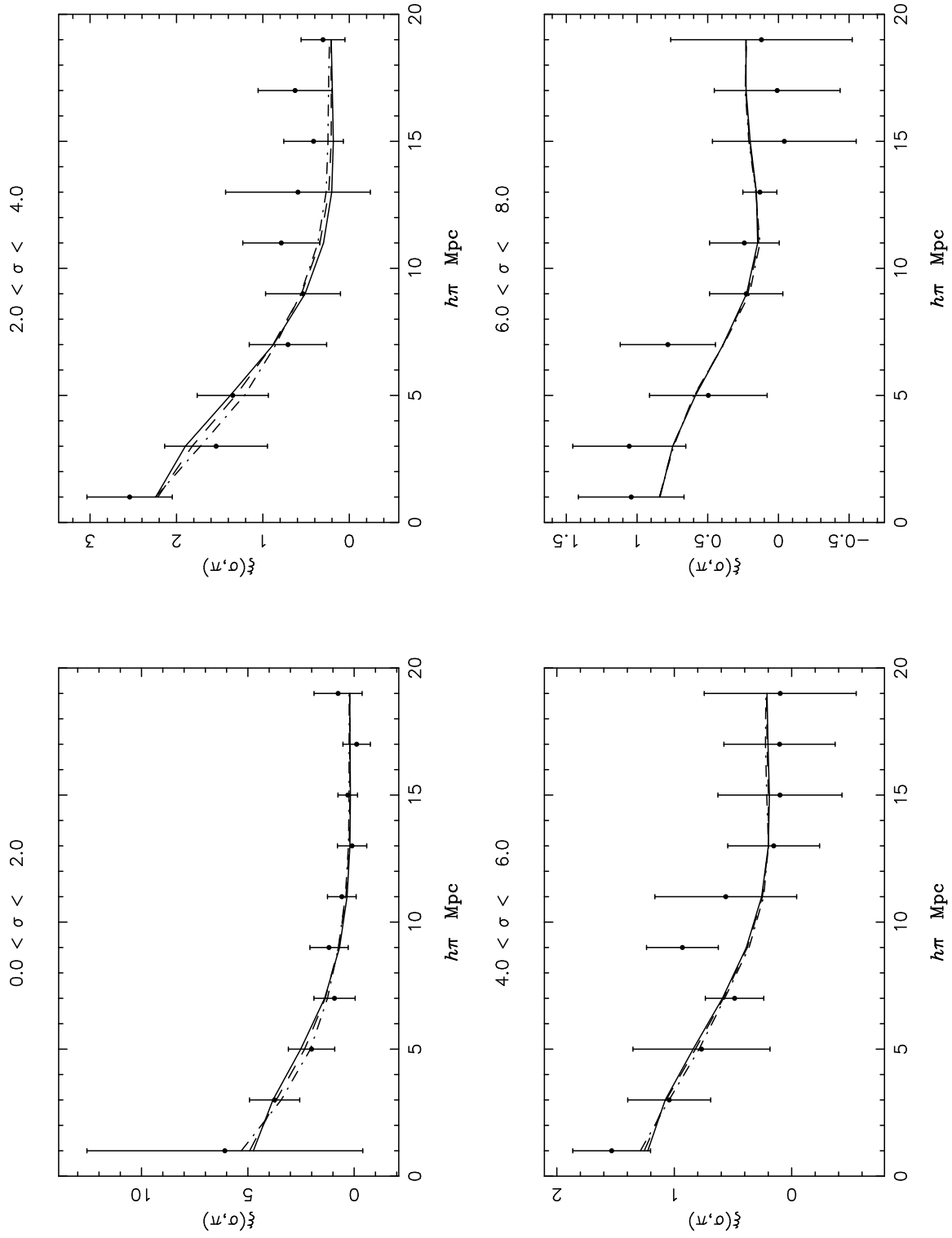


Figure 3: a

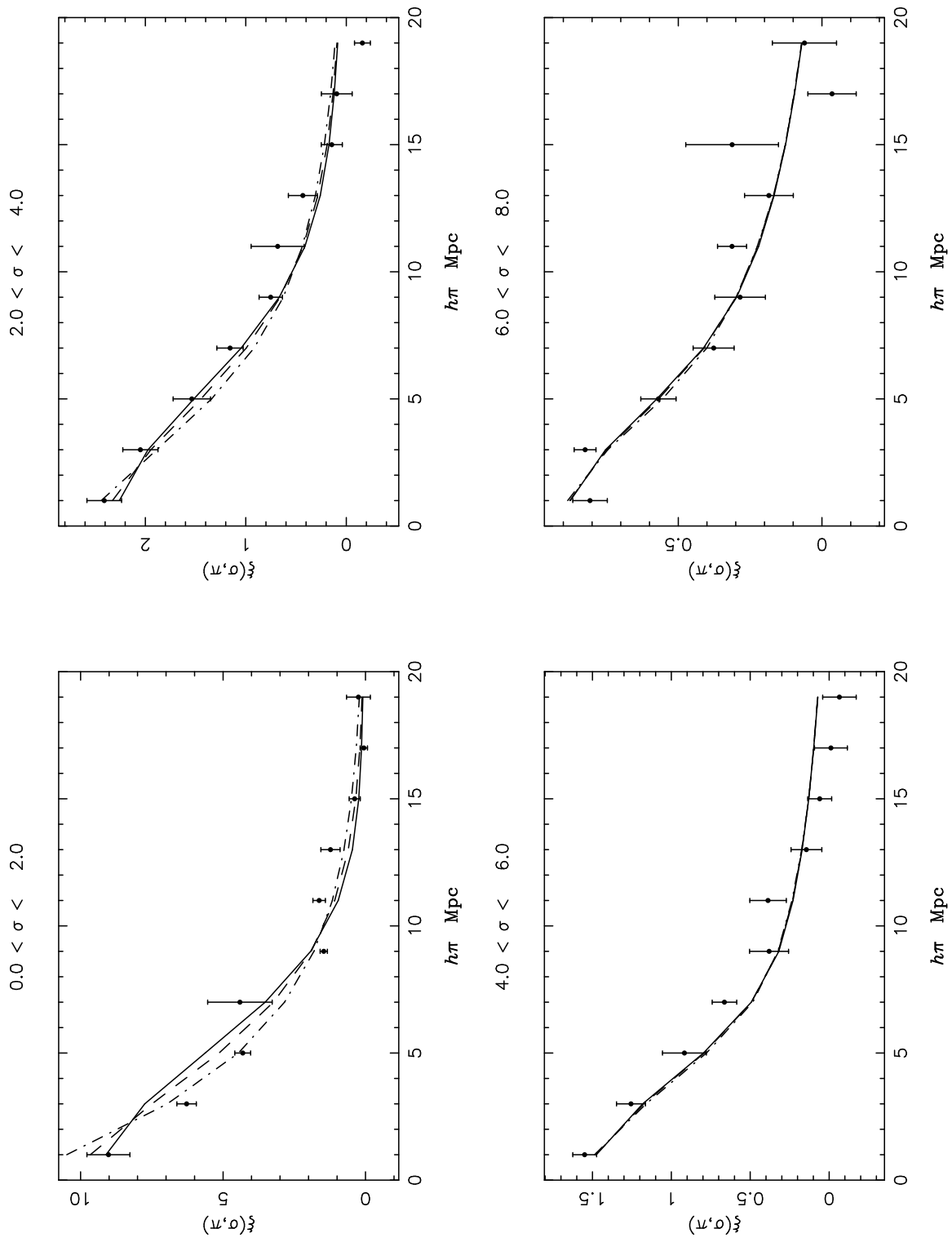


Figure 3: b

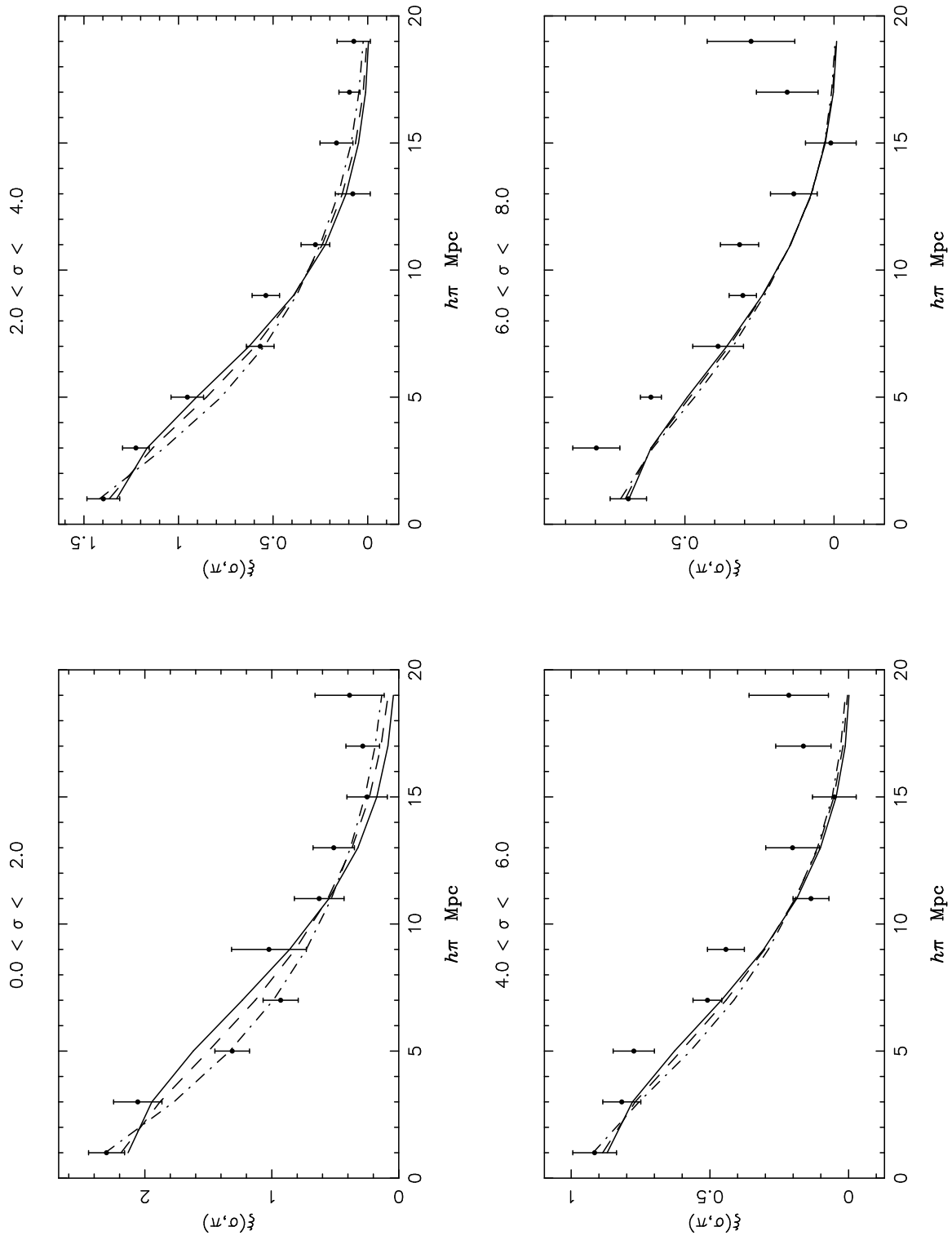


Figure 3: c

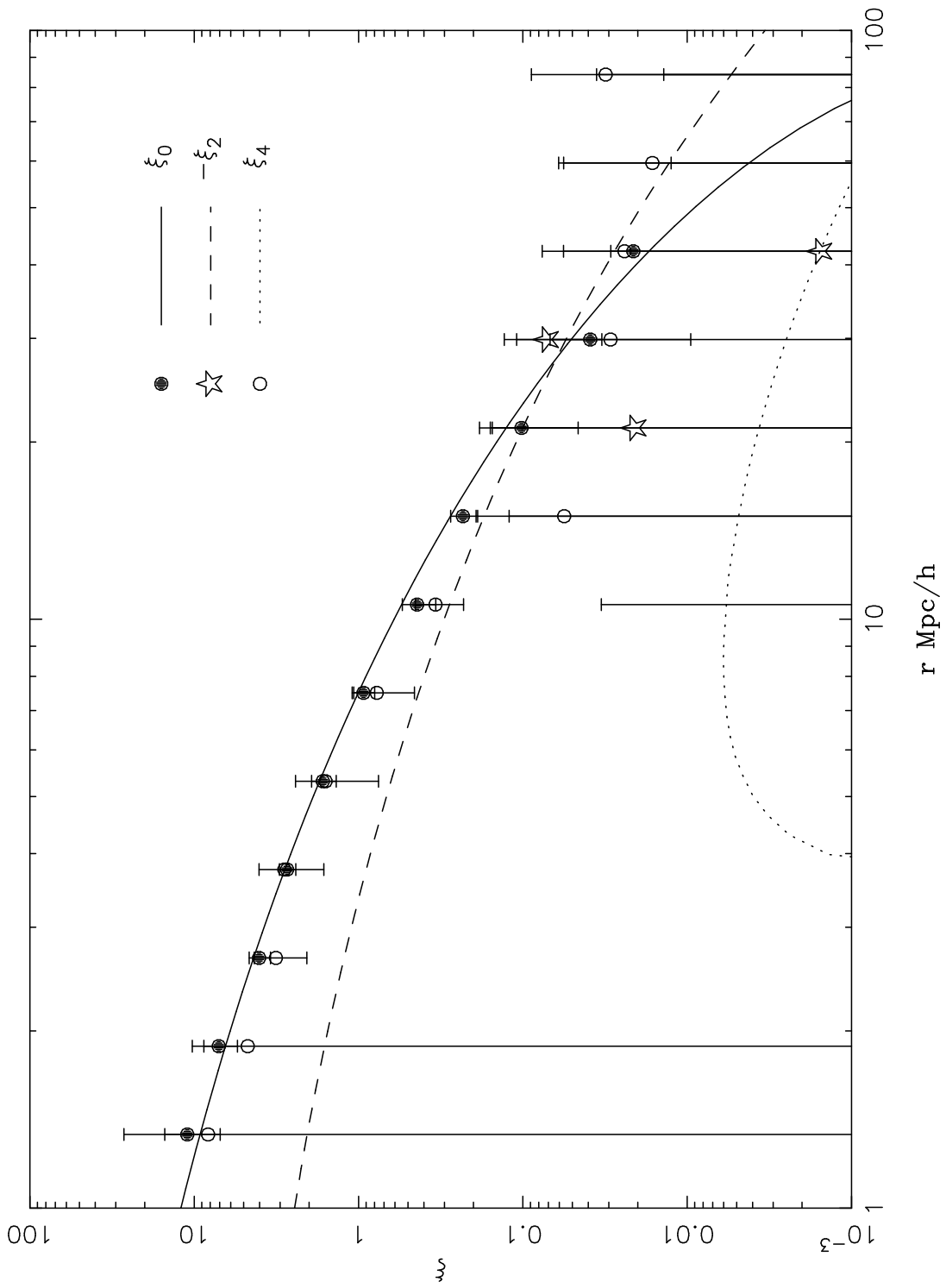


Figure 4: a

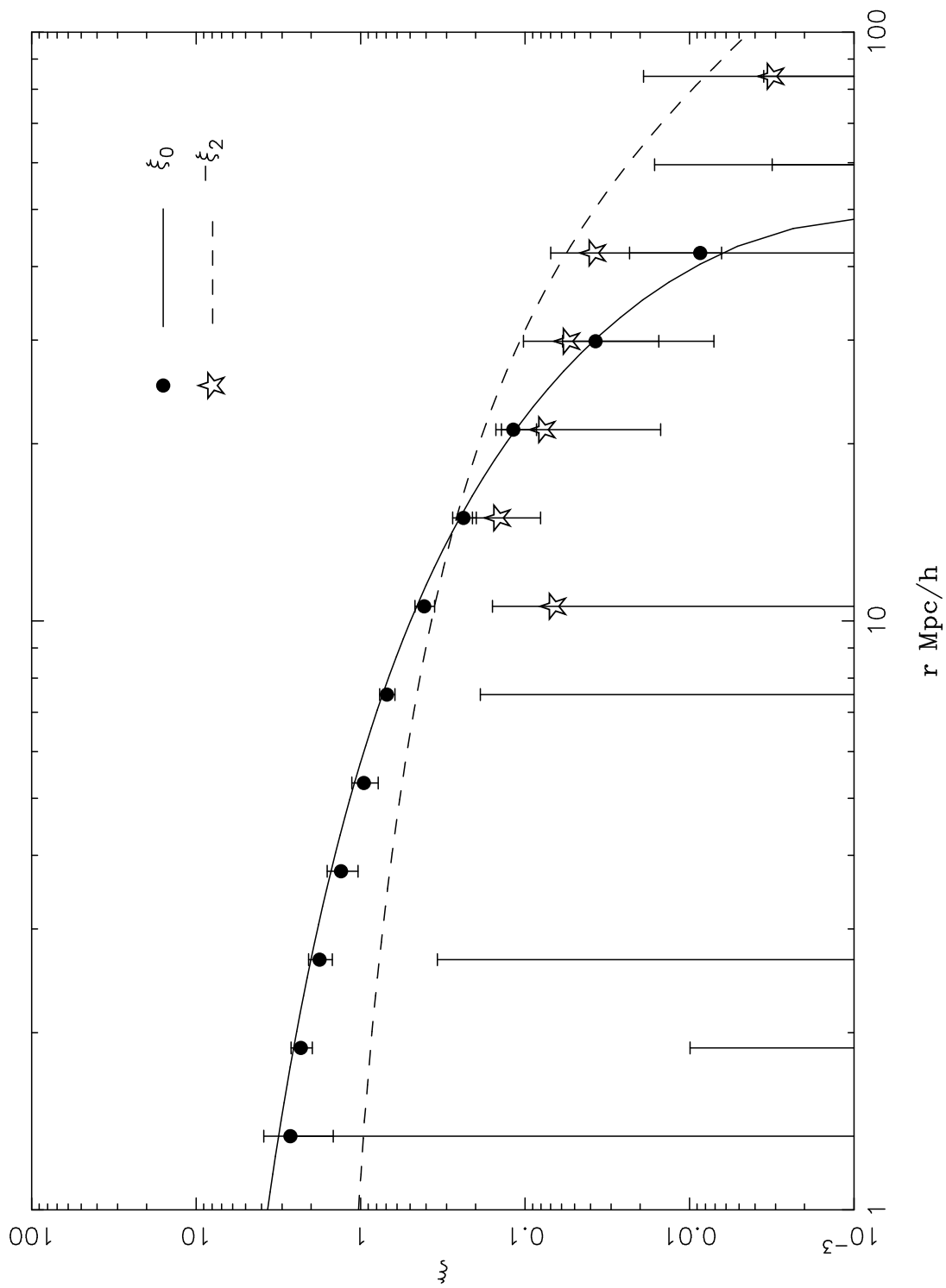


Figure 4: b

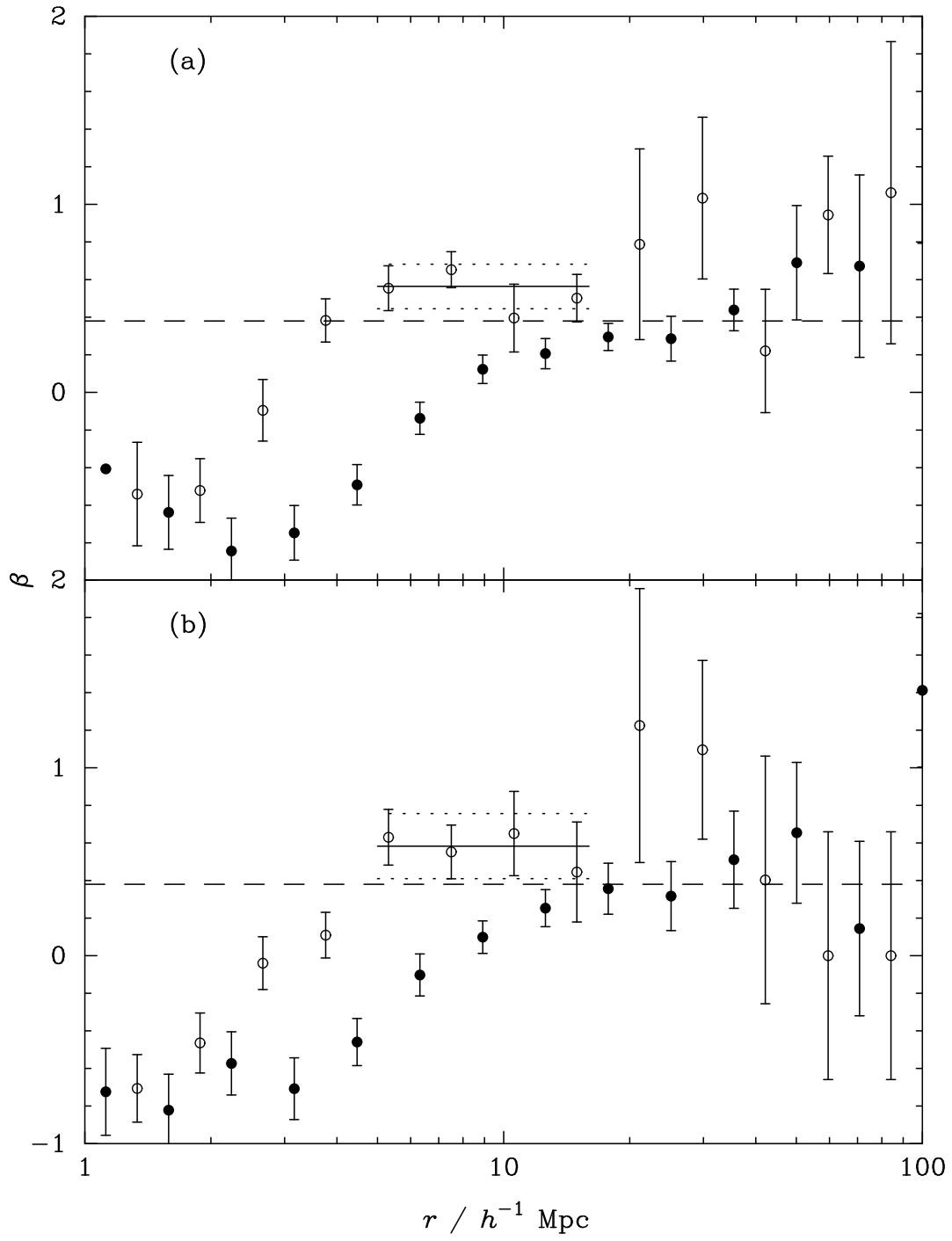


Figure 5:

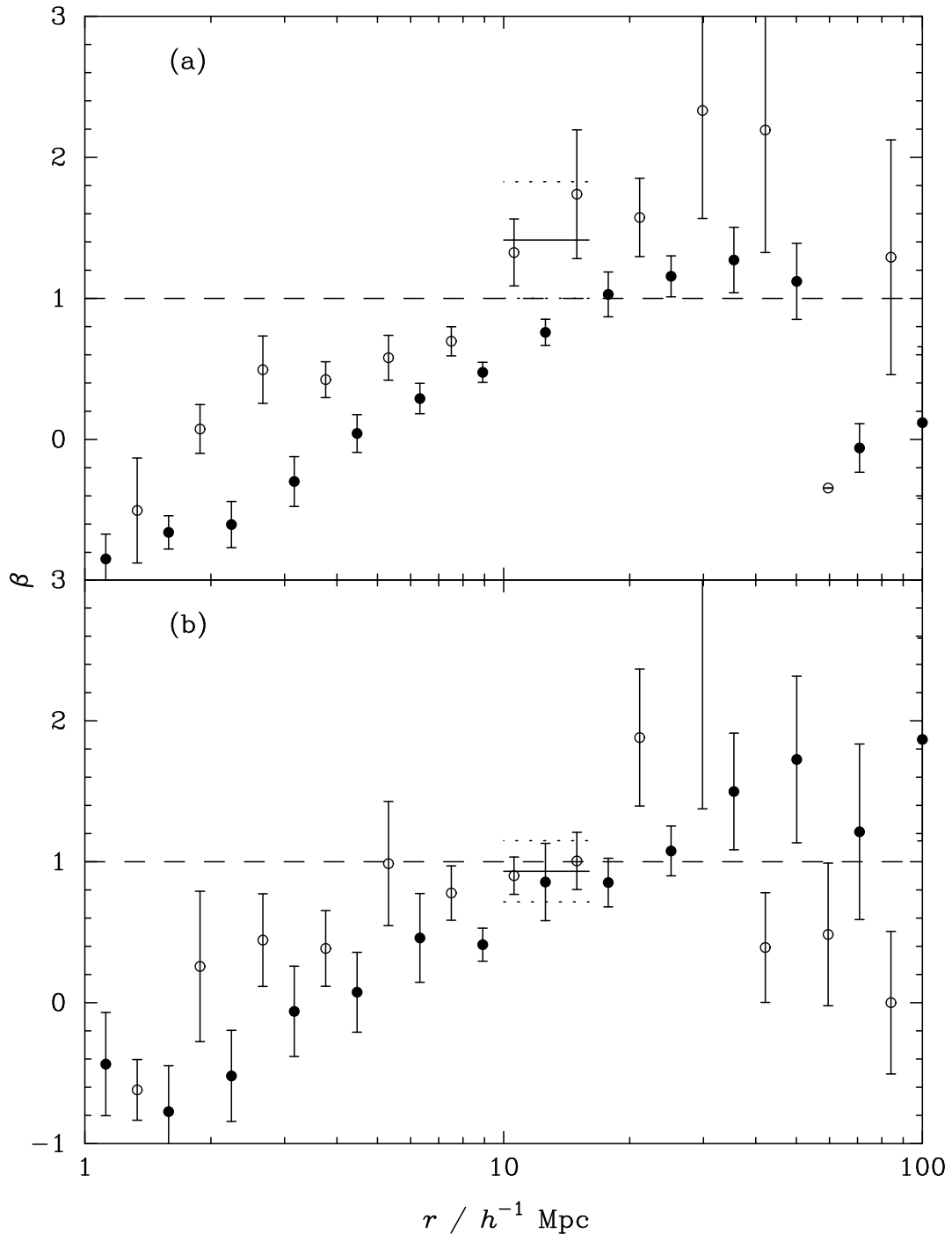


Figure 6:

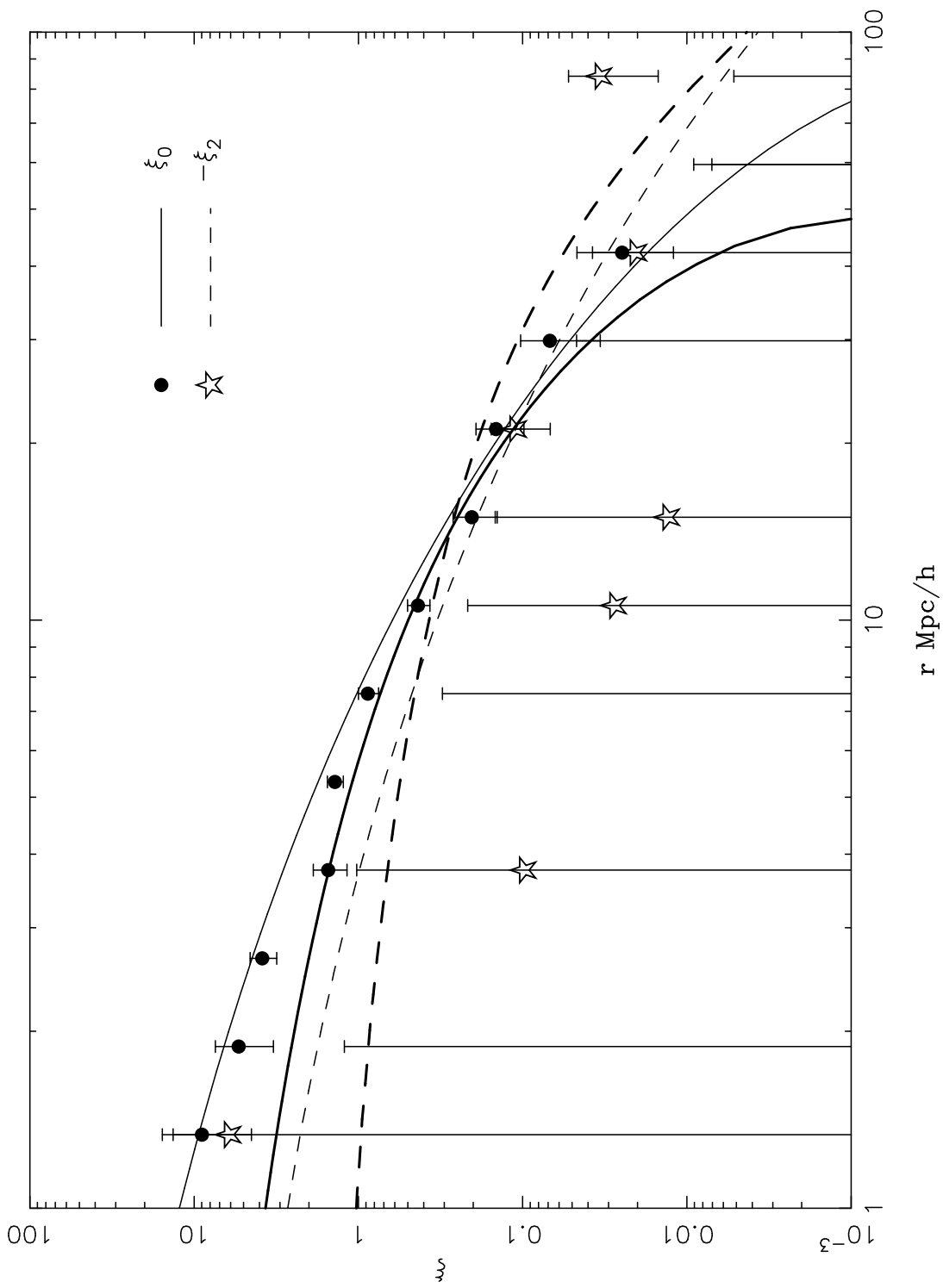


Figure 7:

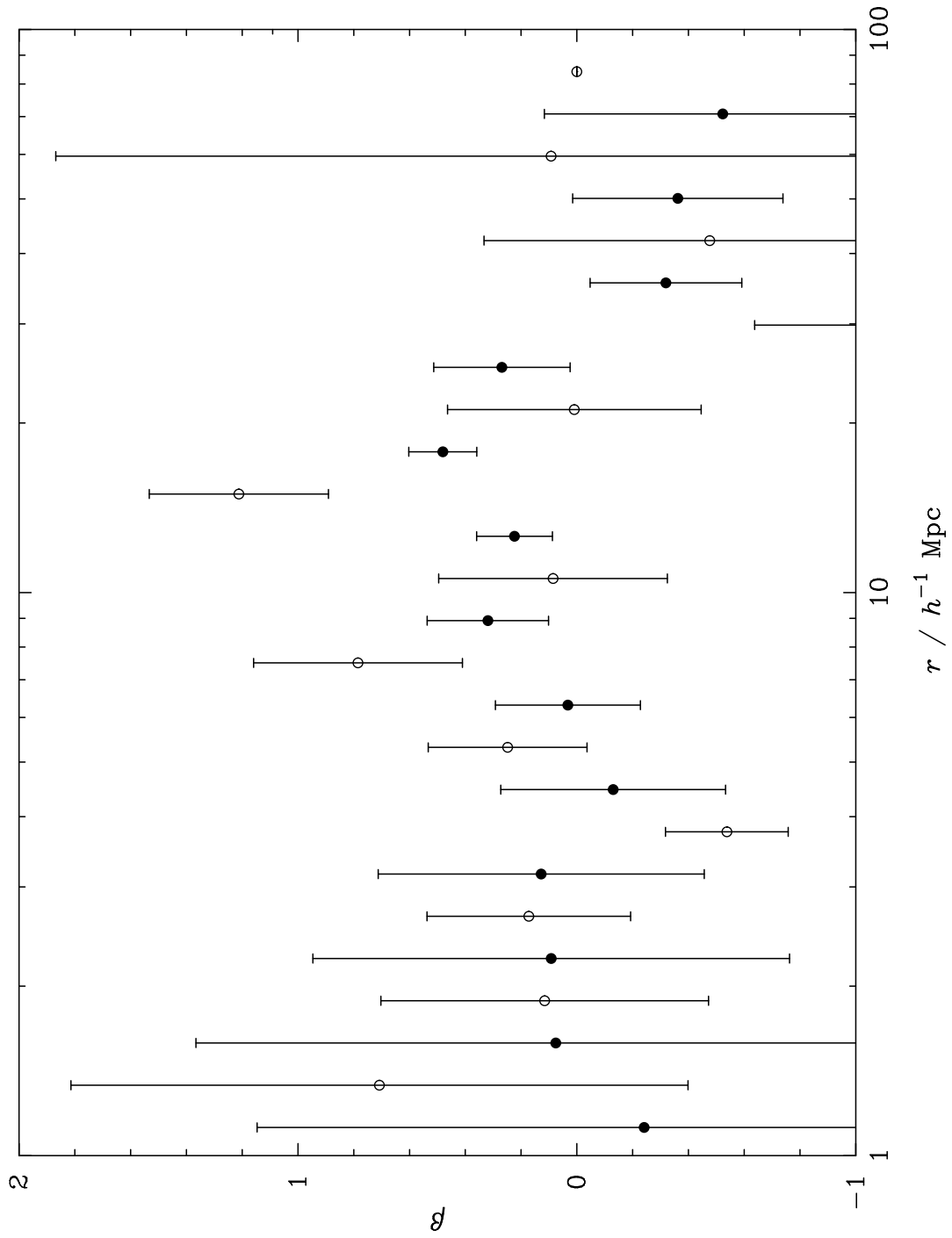


Figure 8:

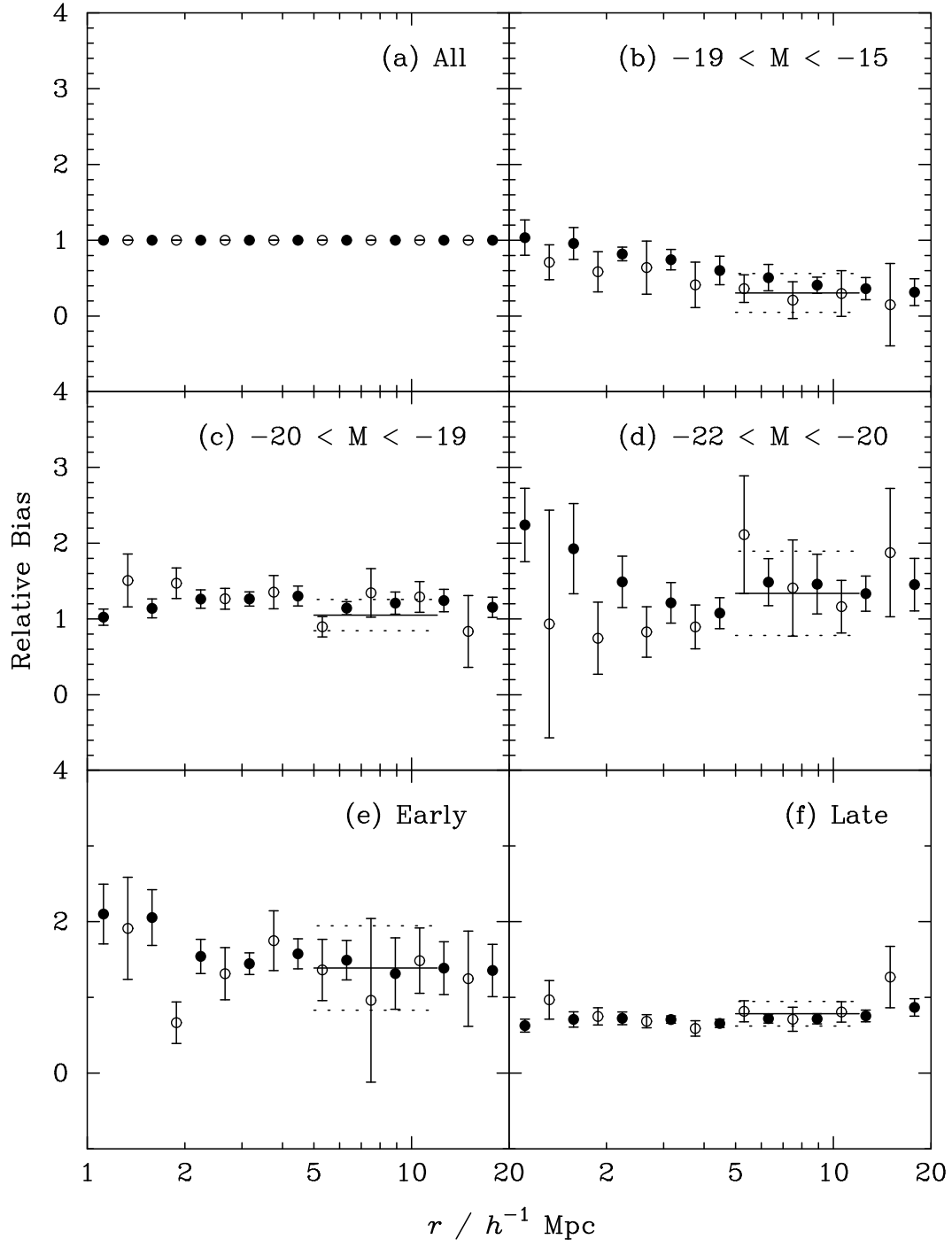


Figure 9:

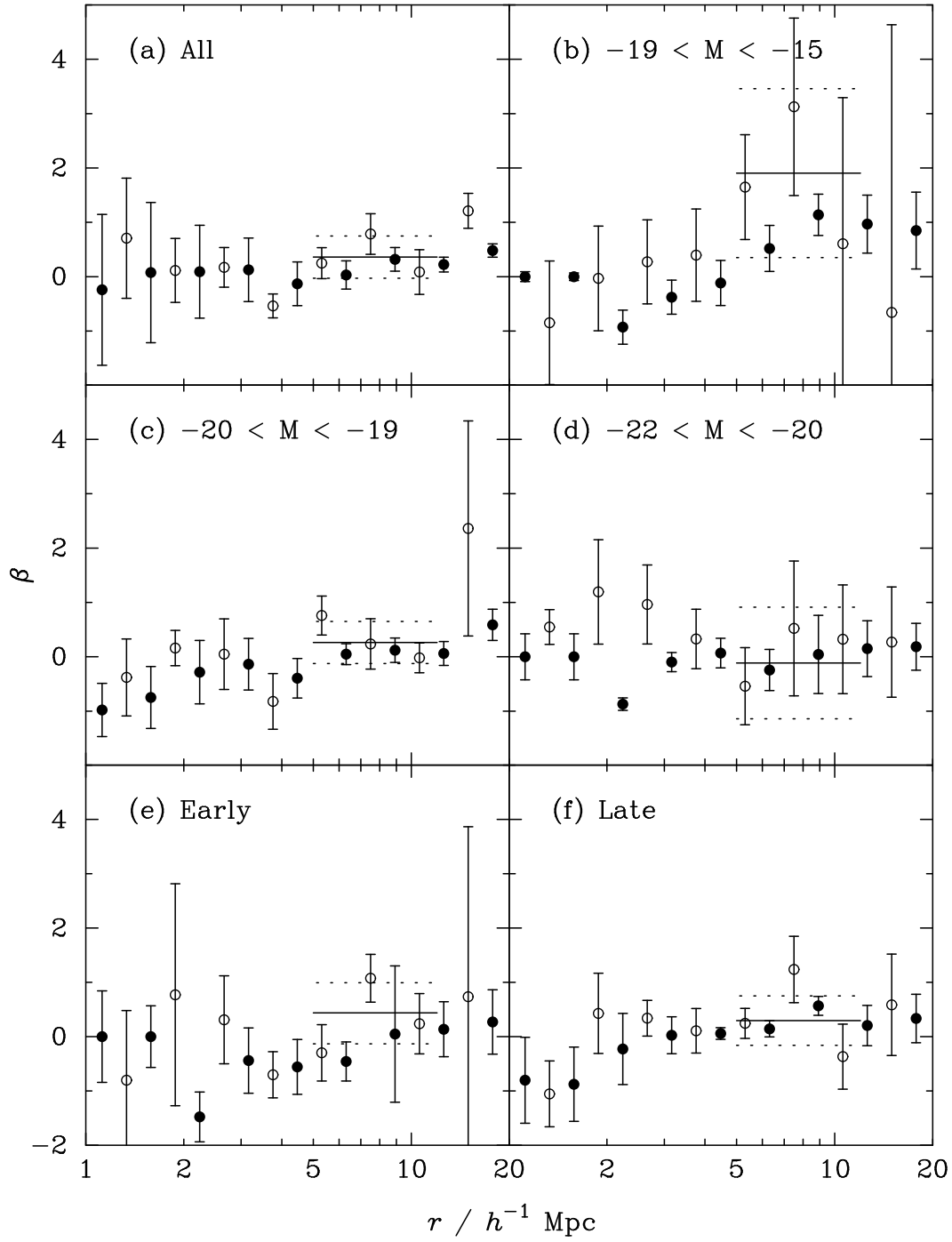


Figure 10: